

pK_a measurements for the SAMPL6 prediction challenge for a set of kinase inhibitor-like fragments

Mehtap Işık^{1,2}, Dorothy Levorse³, Ariën S. Rustenburg^{1,4}, Ikenna E. Ndukwe⁵, Heather Wang⁶, Xiao Wang⁵, Mikhail Reibarkh⁵, Gary E. Martin⁵, Alexey A. Makarov⁶, David L. Mobley⁷, Timothy Rhodes^{3*}, John D. Chodera^{1*}

¹Computational and Systems Biology Program, Sloan Kettering Institute, Memorial Sloan Kettering Cancer Center, New York, NY 10065, United States; ²Tri-Institutional PhD Program in Chemical Biology, Weill Cornell Graduate School of Medical Sciences, Cornell University, New York, NY 10065, United States; ³Pharmaceutical Sciences, MRL, Merck & Co., Inc., 126 East Lincoln Avenue, Rahway, New Jersey 07065, United States; ⁴Graduate Program in Physiology, Biophysics, and Systems Biology, Weill Cornell Medical College, New York, NY 10065, United States; ⁵Process and Analytical Research and Development, Merck & Co., Inc., Rahway, NJ 07065, United States; ⁶Analytical Research & Development, MRL, Merck & Co., Inc., MRL, 126 East Lincoln Avenue, Rahway, New Jersey 07065, United States; ⁷Department of Pharmaceutical Sciences and Department of Chemistry, University of California, Irvine, Irvine, California 92697, United States

***For correspondence:**

timothy_rhodes@merck.com (TR); john.chodera@choderalab.org (JDC)

Abstract Determining the net charge and protonation states populated by a small molecule in an environment of interest or the cost of altering those protonation states upon transfer to another environment is a prerequisite for predicting its physicochemical and pharmaceutical properties. The environment of interest can be aqueous, an organic solvent, a protein binding site, or a lipid bilayer. Predicting the protonation state of a small molecule is essential to predicting its interactions with biological macromolecules using computational models. Incorrectly modeling the dominant protonation state, shifts in dominant protonation state, or the population of significant mixtures of protonation states can lead to large modeling errors that degrade the accuracy of physical modeling. Low accuracy hinders the use of physical modeling approaches for molecular design. For small molecules, the acid dissociation constant (pK_a) is the primary quantity needed to determine the ionic states populated by a molecule in an aqueous solution at a given pH. As a part of SAMPL6 community challenge, we organized a blind pK_a prediction component to assess the accuracy with which contemporary pK_a prediction methods can predict this quantity, with the ultimate aim of assessing the expected impact on modeling errors this would induce. While a multitude of approaches for predicting pK_a values currently exist, predicting the pK_a s of drug-like molecules can be difficult due to challenging properties such as multiple titratable sites, heterocycles, and tautomerization. For this challenge, we focused on set of 24 small molecules selected to resemble selective kinase inhibitors—an important class of therapeutics replete with titratable moieties. Using a Sirius T3 instrument that performs automated acid-base titrations, we used UV absorbance-based pK_a measurements to construct a high-quality experimental reference dataset of macroscopic pK_a s for the evaluation of computational pK_a prediction methodologies that was utilized in the SAMPL6 pK_a challenge. For several compounds in which the microscopic protonation states associated with macroscopic pK_a s were ambiguous, we performed follow-up NMR experiments to disambiguate the microstates involved in the transition. This dataset provides a useful standard benchmark dataset for the evaluation of pK_a prediction methodologies on kinase inhibitor-like compounds.

43

44 **Keywords**

45 acid dissociation constants · spectrophotometric pK_a measurement · blind prediction challenge · SAMPL ·
46 macroscopic pK_a · microscopic pK_a · macroscopic protonation state · microscopic protonation state

47 **Abbreviations**

48 **SAMPL** Statistical Assessment of the Modeling of Proteins and Ligands

49 **pK_a** $-\log_{10}$ acid dissociation equilibrium constant

50 **$p_s K_a$** $-\log_{10}$ apparent acid dissociation equilibrium constant in cosolvent

51 **DMSO** Dimethyl sulfoxide

52 **ISA** Ionic-strength adjusted

53 **SEM** Standard error of the mean

54 **TFA** Target factor analysis

55 **LC-MS** Liquid chromatography - mass spectrometry

56 **NMR** Nuclear magnetic resonance spectroscopy

57 **HMBC** Heteronuclear Multiple-Bond Correlation

58 **TFA-*d*** deuterio-trifluoroacetic acid

59 **Introduction**

60 SAMPL (Statistical Assessment of the Modeling of Proteins and Ligands) is a recurring series of blind prediction
61 challenges for the computational chemistry community [1, 2]. Through these challenges, SAMPL aims to
62 evaluate and advance computational tools for rational drug design. SAMPL has driven progress in a number
63 of areas over seven previous rounds of challenge cycles [3–7, 7–15] by focusing the community on specific
64 phenomena relevant to drug discovery poorly predicted by current models, isolating that phenomenon
65 from other confounding factors in well-designed test systems, evaluating tools prospectively, enabling data
66 sharing to learn from failures, and releasing the resulting high-quality datasets into the community as
67 benchmark sets.

68 As a stepping stone to enabling the accurate prediction of protein-ligand binding affinities, SAMPL
69 has focused on evaluating how well physical and empirical modeling methodologies can predict various
70 physicochemical properties relevant to binding and drug discovery, such as hydration free energies (which
71 model aspects of desolvation in isolation), distribution coefficients (which model transfer from relatively
72 homogeneous aqueous to nonpolar environments), and host-guest binding affinities (which model high-
73 affinity association without the complication of slow protein dynamics). These physicochemical property
74 prediction challenges—in addition to assessing the predictive accuracy of quantities that are useful in various
75 stages of drug discovery in their own right—have been helpful in pinpointing deficiencies in computational
76 models that can lead to substantial errors in affinity predictions.

77 **Neglect of protonation state effects can lead to large modeling errors**

78 As part of the SAMPL5 challenge series, a new cyclohexane-water distribution constant ($\log D$) prediction
79 challenge was introduced, where participants predicted the transfer free energy of small drug-like molecules
80 between an aqueous buffer phase at pH 7.4 and a nonaqueous cyclohexane phase [16, 17]. While octanol-
81 water distribution coefficient measurements are more common, cyclohexane was selected for the simplicity
82 of its liquid phase and relative dryness compared to wet octanol phases. While the expectation was that
83 this challenge would be relatively straightforward given the lack of complexity of cyclohexane phases,
84 analysis of participant performance revealed that multiple factors contributed to significant prediction
85 failures: poor conformational sampling of flexible solute molecules, misprediction of relevant protonation
86 and tautomeric states (or failure to accommodate shifts in their populations), and force field inaccuracies
87 resulting in bias towards the cyclohexane phase. While these findings justified the benefit of future iterations
88 of blind distribution or partition coefficient challenges, the most surprising observation from this initial $\log D$
89 challenge was that participants almost uniformly neglected to accurately model protonation state effects,

90 and that neglect of these effects led to surprisingly large errors in transfer free energies [16–18]. Careful
91 quantum chemical assessments of the magnitude of these protonation state effects found that their neglect
92 could introduce errors up to 6–8 kcal/mol for some compounds [18]. This effect stems from the need to
93 account for the free energy difference between the major ionization state in cyclohexane (most likely neutral
94 state) and in water phase (which could be neutral or charged).

95 To isolate these surprisingly large protonation state modeling errors from difficulties related to lipophilic-
96 ity ($\log P$ and $\log D$) prediction methods, we decided to organize a set of staged physicochemical property
97 challenges using a consistent set of molecules that resemble small molecule kinase inhibitors—an important
98 drug class replete with multiple titratable moieties. This series of challenges will first evaluate the ability
99 of current-generation modeling tools to predict acid dissociation constants (pK_a). It will be followed by a
100 partition/distribution coefficient challenge to evaluate the ability to incorporate experimentally-provided
101 pK_a values into prediction of distribution coefficients to ensure methodologies can correctly incorporate
102 protonation state effects into their predictions. A third challenge stage will follow: a new blinded parti-
103 tion/distribution coefficient challenge where participants must predict pK_a values on their own. At the
104 conclusion of this series of challenges, we will ensure that modern physical and empirical modeling methods
105 have eliminated this large source of spurious errors from modeling both simple and complex phenomena.

106 This article reports on the experiments for the first stage of this series of challenges: SAMPL6 pK_a
107 prediction challenge. The selection of a small molecule set and collection of experimental pK_a data are
108 described in detail.

109 Conceptualization of a blind pK_a challenge

110 This is the first time a blind pK_a prediction challenge has been fielded as part of SAMPL. In this first iteration of
111 the challenge, we aimed to assess the performance of current pK_a prediction methods and isolate potential
112 causes of inaccurate pK_a estimates.

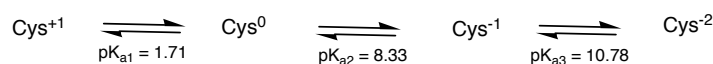
113 The prediction of pK_a values for drug-like molecules can be complicated by several effects: the presence
114 of multiple (potentially coupled) titratable sites, the presence of heterocycles, tautomerization, the confor-
115 mational flexibility of large molecules, and ability of intramolecular hydrogen bonds to form. We decided
116 to focus on the chemical space of small molecule kinase inhibitors in the first iteration of pK_a prediction
117 challenge. A total of 24 small organic molecules (17 drug-fragment-like and 7 drug-like) were selected for
118 their similarity to known small molecule kinase inhibitors, while also considering properties predicted to
119 affect the experimental tractability of pK_a and $\log P$ measurements such as solubility and predicted pK_a s.
120 Macroscopic pK_a values were collected experimentally with UV-absorbance spectroscopy-based pK_a mea-
121 surements using a Sirius T3 instrument, which automates the sample handling, titration, and spectroscopic
122 measurements to allow high-quality pK_a determination. The Sirius T3 is equipped with an autosampler
123 which allowed us to run 8–10 measurements per day. Experimental data were kept blinded for three months
124 (25 Oct 2017 through 23 Jan 2018) to allow participants in the SAMPL6 pK_a challenge to submit truly blinded
125 computational predictions. Eleven research groups participated in this challenge, providing a total of 93
126 prediction submission sets that cover a large variety of contemporary pK_a prediction methods.

127 Our selected experimental approach determines macroscopic pK_a values

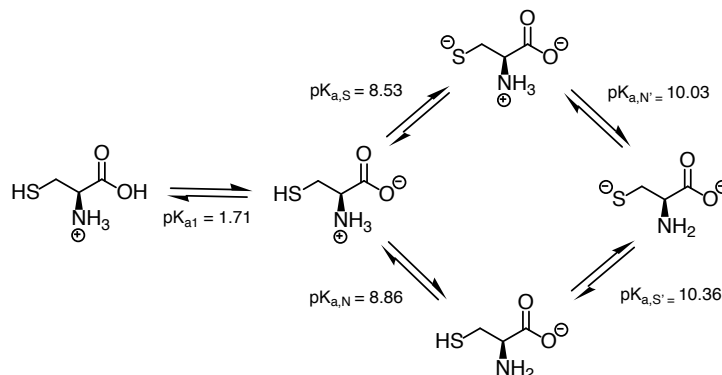
128 Whenever experimental pK_a measurements are used for evaluating pK_a predictions, it is important to
129 differentiate between microscopic and macroscopic pK_a values. In molecules containing multiple titratable
130 moieties, the protonation state of one group can affect the proton dissociation propensity of another
131 functional group. In such cases, the **microscopic pK_a** (group pK_a) refers to the pK_a of deprotonation of
132 a single titratable group while all the other titratable and tautomerizable functional groups of the same
133 molecule are held fixed. Different protonation states and tautomer combinations constitute different
134 microstates. The **macroscopic pK_a** (molecular pK_a) defines the acid dissociation constant related to the
135 observable loss of a proton from a molecule regardless of which functional group the proton is dissociating
136 from, so it doesn't necessarily convey structural information.

137 Whether a measured pK_a is microscopic or macroscopic depends on the experimental method used
138 (Figure 2). For a molecule with only one titratable proton, the microscopic pK_a is equal to the macroscopic

Macroscopic pK_a s of Cysteine



Microscopic pK_a s of Cysteine



pK_a s of Glycine

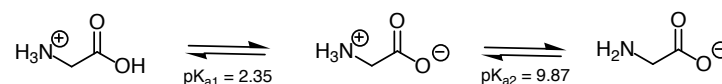


Figure 1. Assignment of cysteine and glycine pK_a values. pK_{a1} , pK_{a2} , and pK_{a3} are macroscopic acid dissociation constants for cysteine and glycine [24]. When pK_a values of a polyprotic molecule are very different, such as in the case of glycine, it is possible to assign the pK_a s to individual groups since the dissociation of protons is stepwise [19]. However, stepwise dissociation cannot be assumed for cysteine, because pK_{a2} and pK_{a3} are very close in value. Four underlying microscopic pK_a s ($pK_{a,S}$, $pK_{a,N}$, $pK_{a,S'}$, and $pK_{a,N'}$) for cysteine were measured using UV spectra analysis of cysteine and derivatives [25]. Notice that the proximity of $pK_{a,S}$ and $pK_{a,N}$ values indicates similar probability of proton dissociation from these groups. This figure is adopted from [19].

139 pK_a . For a molecule with multiple titratable groups, however, throughout a titration from acidic to basic pH,
 140 the deprotonation of some functional groups can take place almost simultaneously. For these multiprotic
 141 molecules, the experimentally-measured macroscopic pK_a will include contributions from multiple micro-
 142 scopic pK_a s with similar values (i.e., acid dissociation of multiple microstates). Cysteine provides an example
 143 of this behavior with its two macroscopic pK_a s observable by spectrophotometric or potentiometric pK_a
 144 measurement experiments [19, 20].

145 While four microscopic pK_a s can be defined for cysteine, experimentally observed pK_a values cannot
 146 be assigned to individual functional groups directly (Figure 1, top). More advanced techniques capable of
 147 resolving individual protonation sites—such as NMR [21], Raman spectroscopy [22, 23], and the analysis of
 148 pK_a s in molecular fragments or derivatives—are required to unambiguously assign the site of protonation
 149 state changes. On the other hand, when there is a large difference between microscopic pK_a s in a multiprotic
 150 molecule, the proton dissociations won't overlap and macroscopic pK_a s observed by experiments can be
 151 assigned to individual titratable groups. The pK_a values of glycine provide a good example of this scenario
 152 (Figure 1, bottom) [19, 20, 22]. We recommend the short review on the assignment of pK_a values authored by
 153 Ivan G. Darvey [20] for a good introduction to the concepts of macroscopic vs microscopic pK_a values.

154 The most common methods for measuring small molecule pK_a s are UV-absorbance spectroscopy (UV-
 155 metric titration) [28–30], potentiometry (pH-metric titration) [30, 31], capillary electrophoresis [32, 33],
 156 and NMR spectroscopy [21], with NMR being the most time-consuming approach. Other, less popular
 157 pK_a measurement techniques include conductometry, HPLC, solubility or partition based estimations,
 158 calorimetry, fluorometry, and polarimetry [34]. UV-metric and pH-metric methods (Figure 3) of Sirius T3 are

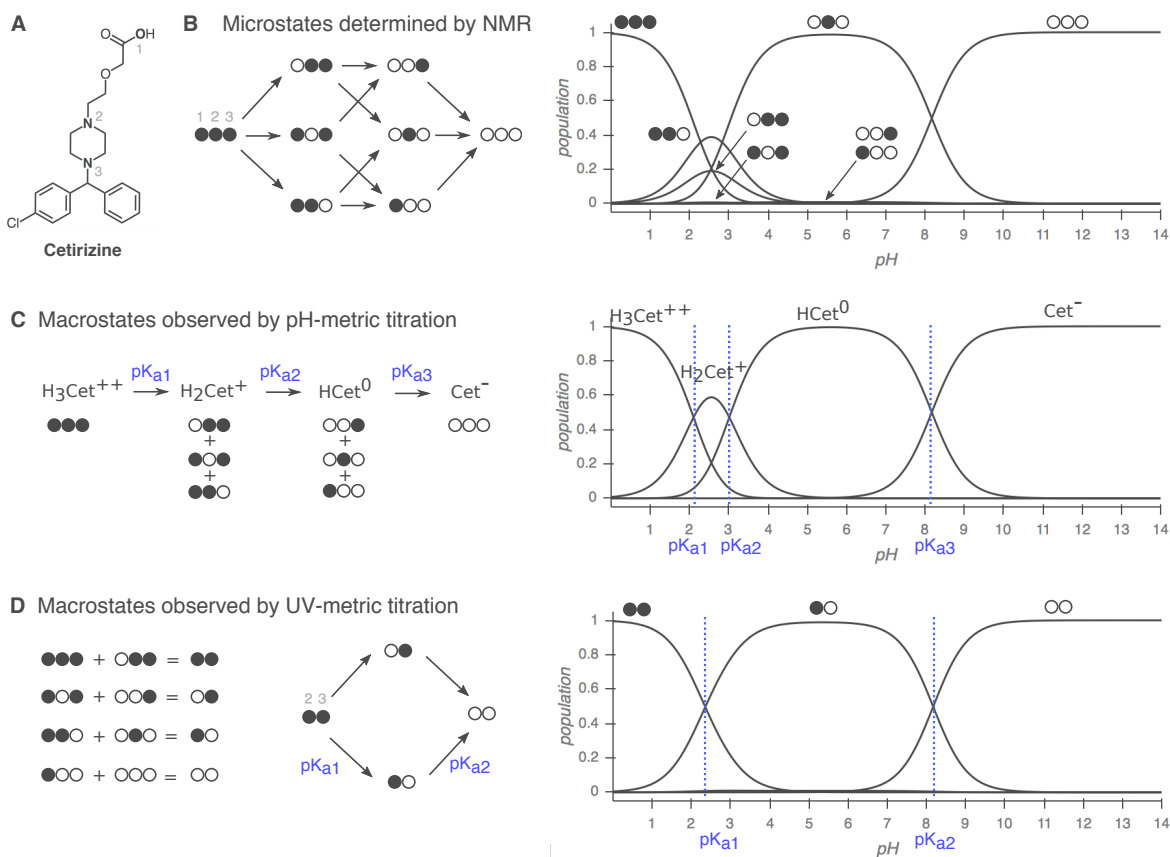


Figure 2. Comparison of macroscopic and microscopic pK_a measurement methods. Filled circles represent protonated sites and empty circles represent deprotonated sites with the order of carboxylic acid (1), piperazine nitrogen (2), and piperazine nitrogen (3). Protonation state populations shown for pH-metric and UV-metric pK_a measurement methods are simulations, calculated using NMR-based microscopic pK_a values. **(A)** Cetirizine has $n = 3$ titratable sites, shown in bold. **(B) Left:** The 8 microstates (2^n) and 12 microscopic pK_a s ($n2^{n-1}$) of cetirizine. **Right:** Relative population of microspecies with respect to pH. Potentially all microstates can be resolved via NMR. **(C)** Simulated pH-metric (potentiometric) titration and macroscopic populations. For a polyprotic molecule, only macroscopic pK_a s can be measured with pH-metric titration. Microstates with different total charge (related to the number of protons) can be resolved, but microstates with the same total charge are observed as one macroscopic population. **(D)** Simulated microscopic populations for UV-metric (spectrophotometric) titration of cetirizine. Since only protonation of the titration sites within four heavy atoms of the UV-chromophore is likely to cause an observable change in the UV-absorbance spectra, microstates that only differ by protonation of the distal carboxylic acid cannot be differentiated. Moreover, populations that overlap may or may not be resolvable depending on how much their absorbance spectra in the UV region differ. Both UV-metric and pH-metric pK_a determination methods measure macroscopic pK_a s for polyprotic molecules, which cannot easily be assigned to individual titration sites and underlying microstate populations in the absence of other experimental evidence that provides structural resolution, such as NMR. Note that macroscopic populations observed in these two methods are composed of different combinations of microstates depending on the principles of measurement technique. Here, the illustrative diagram style was adopted from [26], and NMR-determined microscopic pK_a s for cetirizine were taken from [27].

159 limited to measuring aqueous pK_a values between 2 and 12 due to limitations of the pH electrode used in
160 these measurements. The pH-metric method relies on determining the stoichiometry of bound protons
161 with respect to pH, calculated from volumetric titration with acid or base solutions. Accurate pH-metric
162 measurements require high concentrations of analyte as well as analytically prepared acid/base stocks
163 and analyte solutions. By contrast, UV-metric pK_a measurements rely on the differences in UV absorbance
164 spectra of different protonation states, generally permitting lower concentrations of analyte to be used. The
165 pH and UV absorbance of the analyte solution are monitored during titration.

166 Both UV-metric and pH-metric pK_a determination methods measure macroscopic pK_a s for polyprotic
167 molecules, which cannot be easily assigned to individual titration sites and underlying microstate popu-
168 lations in the absence of other experimental evidence that provides structural information, such as NMR
169 (Figure 2). Macroscopic populations observed in these two methods are composed of different combinations
170 of microstates depending on the principles of measurement technique. In potentiometric titrations, mi-
171 crostates with same total charge will be observed as one macrostate, while in spectrophotometric titrations,
172 protonation sites remote from chromophores might be spectroscopically invisible, and macrostates will be
173 formed from collections of microstates that manifest similar UV-absorbance spectra.

174 For UV-metric method to resolve populations of microstates, sufficiently different UV spectra between
175 microstates and sufficiently non-overlapping change of populations with respect to pH are needed. However,
176 relative tautomer populations of microstates with the same total charge do not depend on pH and stay
177 constant while pH is titrated (Figure 2B), therefore they cannot be resolved by UV-metric method. The
178 pH-metric method also cannot resolve microstates that have the same total charge as shown in Figure 2C.

179 Spectrophotometric pK_a determination is more sensitive than potentiometric determination, requiring
180 low analyte concentrations (50–100 μ M)—especially advantageous for compounds with low solubilities—
181 but is only applicable to titration sites near chromophores. For protonation state changes to affect UV
182 absorbance, a useful rule of thumb is that the protonation site should be a maximum of four heavy atoms
183 away from the chromophore, which might consist of conjugated double bonds, carbonyl groups, aromatic
184 rings, etc. Although potentiometric measurements do not suffer from the same observability limitations,
185 higher analyte concentrations (\sim 5 mM) are necessary for the analyte to provide sufficiently large enough
186 buffering capacity signal above water to produce an accurate measurement. The accuracy of pK_a s fit to
187 potentiometric titrations can also be sensitive to errors in the estimated concentration of the analyte in the
188 sample solution, while UV-metric titrations are insensitive to concentration errors. We therefore decided to
189 adopt spectrophotometric measurements for collecting the experimental pK_a data for this challenge, and
190 selected a compound set to ensure that all potential titration sites are in the vicinity of UV chromophores.

191 Here, we report on the selection of SAMPL6 pK_a challenge compounds, their macroscopic pK_a values
192 measured by UV-metric titrations using a Sirius T3, as well as NMR-based microstate characterization of two
193 SAMPL6 compounds with ambiguous protonation states associated with the observed macroscopic pK_a s
194 (SM07 and SM14). We discuss implications of the use of this experimental technique for the interpretation
195 of pK_a data, and provide suggestions for future pK_a data collection efforts with the goal of evaluating or
196 training computational pK_a predictions.

197 **Methods**

198 **Compound selection and procurement**

199 To select a set of small molecules focusing on the chemical space representative of kinase inhibitors for
200 physicochemical property prediction challenges (pK_a and lipophilicity) we started from the kinase-targeted
201 subclass of the ZINC15 chemical library [35] and applied a series of filtering and selection rules as depicted
202 in Figure 4A. We focused on the availability "now" and reactivity "anodyne" subsets of ZINC15 in the first
203 filtering step [<http://zinc15.docking.org/subclasses/kinase/substances/subsets/now+anodyne/>]. The "now"
204 label indicates the compounds were available for immediate delivery, while the "anodyne" label excludes
205 compounds matching filters that flag compounds with the potential for reactivity or pan-assay interference
206 (PAINs) [36, 37].

207 Next, we identified resulting molecules that were also available for procurement through eMolecules [38]

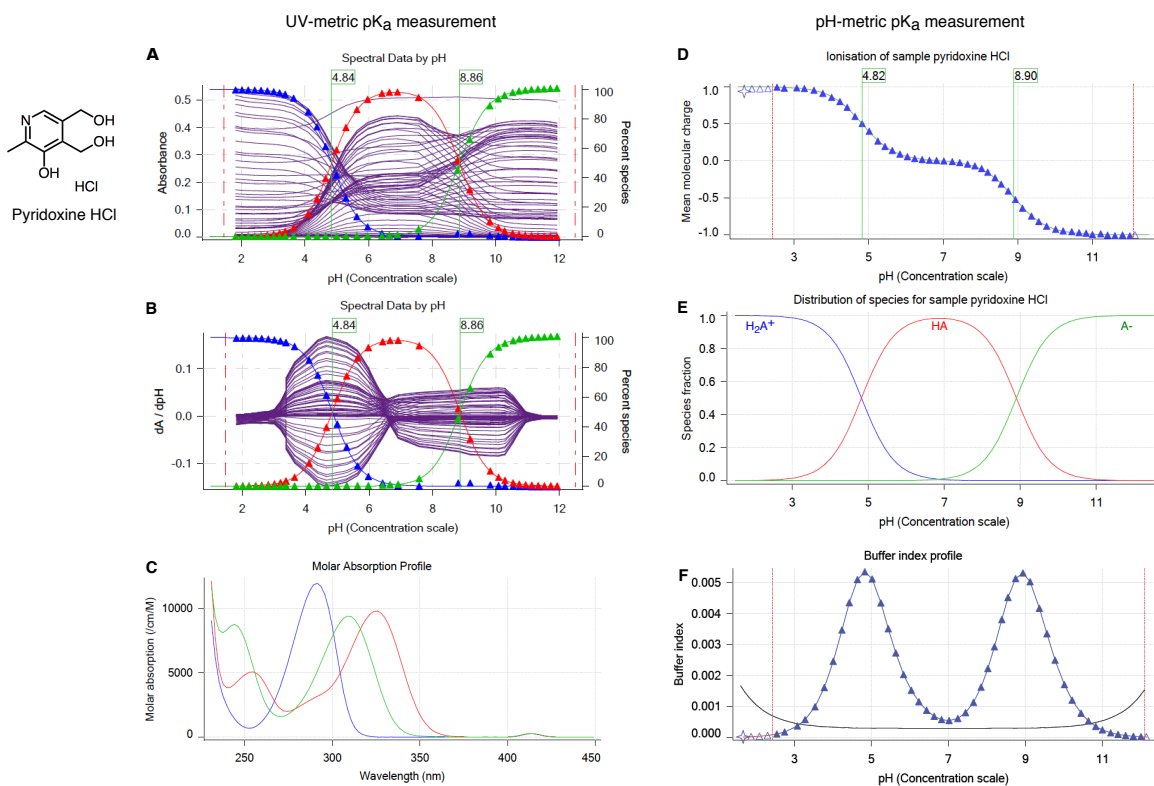


Figure 3. UV-metric (spectrophotometric) and pH-metric (potentiometric) pK_a measurements of pyridoxine HCl with Sirius T3. Spectrophotometric pK_a measurement (panels **A**, **B**, **C**) relies on differences in the UV absorbance spectra between microscopic protonation states to deconvolute the population of macrostate species as a function of pH. While highly sensitive (and therefore requiring a very low analyte concentration of $\sim 50 \mu\text{M}$), this approach can only resolve changes in protonation states for titratable sites near chromophores and cannot separate the populations of microstates that change in the same manner as a function of pH. (**A**) Multiwavelength UV absorbance vs pH. Purple lines represent absorbance at distinct wavelengths in UV region. (**B**) Derivative of multiwavelength absorbance with respect to pH (dA/dpH) vs pH is plotted with purple lines. In **A** and **B**, blue, red, and green triangles represent population of protonation states (from most protonated to least protonated) as calculated from a global fit to experimental UV absorbances for all pH values, while thin lines denote model fits that utilize the fitted model pK_a s to compute populations. pK_a values (green flags) correspond to inflection point of multiwavelength absorbance data where change in absorbance with respect to pH is maximum. (**C**) Molar absorption coefficients vs wavelength for each protonation state as resolved by TFA. **D**, **E**, **F** illustrate potentiometric pK_a measurement where molar addition of acid or base is tracked as pH is titrated. (**D**) Mean molecular charge vs pH. Mean molecular charge is calculated based on the model provided for the analyte: predicted number and nature of titratable sites (acid or base type), and number of counter ions present. pK_a values are calculated as inflection points of charge vs pH plot. (**E**) Predicted macroscopic protonation state populations vs pH calculated based on pK_a values (H_2A^+ : blue, HA: red, and A^- : green) (**F**) Buffering index vs pH profile of water (grey solid line, theoretical) and the sample solution (blue triangles represent experimental data points). A higher concentration of analyte ($\sim 5 \text{ mM}$) is necessary for the potentiometric method than the spectrophotometric method in order to provide large enough buffering capacity signal above water for an accurate measurement.

208 (free version, downloaded 1 June 2017), the supplier that would be used for procurement in this exercise. To
209 find the intersection of ZINC15 kinase subset and eMolecules database, we matched molecules using their
210 canonical isomeric SMILES strings, as computed via the OpenEye OEChem Toolkit (version 2017.Feb.1) [39].

211 To extract availability and price information from eMolecules, we queried using a list of SMILES (as
212 reported in eMolecules database) of the intersection set. We further filtered the intersection set (1204
213 compounds) based on delivery time (Tier 1 suppliers, two-week delivery) and at least 100 mg availability in
214 powder form (format: Supplier Standard Vial). We aimed to purchase 100 mg of each compound in powder
215 form with at least 90% purity. We calculated 100 mg was enough for optimization and replicate experiments
216 to measure pK_a , $\log P$, and solubility measurements with the Sirius T3. Each UV-metric and pH-metric pK_a
217 measurement requires a minimum of 0.01 mg and 1.00 mg compound (solid or delivered via DMSO stock
218 solution), respectively. $\log P$ and pH-dependent solubility measurements require around 2 mg and 10 mg of
219 solid chemical, respectively.

220 Filtering for predicted measurable pK_a s and lack of experimental data

221 The Sirius T3 (Pion) instrument used to collect pK_a and $\log P/\log D$ measurements requires a titratable group
222 in the pK_a range of 2–12, so we aimed to select compounds with predicted pK_a s in the range of 3–11 to allow a
223 ~ 1 pK unit margin of error in pK_a predictions. pK_a predictions for compound selection were calculated using
224 Epik (Schöndinger) sequential pK_a prediction (scan) [40, 41] with target pH 7.0 and tautomerization allowed
225 for generated states. We filtered out all compounds that did not have any predicted pK_a s between 3–11, as
226 well as compounds with two pK_a values predicted to be less than 1 pK_a unit apart in the hopes that individual
227 pK_a s of multiprotic compounds could be resolved with spectrophotometric pK_a measurements. With the
228 goal of selecting compounds suitable for subsequent $\log P$ measurements, we eliminated compounds
229 with OpenEye XlogP [42] values less than -1 or greater than 6. Subsets of compounds with molecular
230 weights between 150–350 g/mol and 350–500 g/mol were selected for fragment-like and drug-like categories
231 respectively. Compounds without available price or stock quantity information were eliminated. As the goal
232 was to provide a blind challenge, compounds with publicly available experimental $\log P$ measurements were
233 also removed. The sources we checked for publicly available experimental $\log P$ values were the following:
234 DrugBank [43] (queried with eMolecules SMILES), ChemSpider [44] (queried by canonical isomeric SMILES),
235 NCI Open Database August 2006 release [45], Enhanced NCI Database Browser [46] (queried with canonical
236 isomeric SMILES), and PubChem [47] (queried with InChIKeys generated from canonical isomeric SMILES
237 with NCI CACTUS Chemical Identifier Resolver [48]).

238 Filtering for kinase inhibitor-like scaffolds

239 In order to include common scaffolds found in kinase inhibitors, we analyzed the frequency of rings
240 found in FDA-approved kinase inhibitors via Bemis-Murcko fragmentation using OMedChem Toolkit of
241 OpenEye [49, 50]. Heterocycles found more than once in FDA-approved kinase inhibitors are shown in
242 Figure 4B. In selecting 25 compounds for the fragment-like set and 10 compounds for the drug-like set, we
243 prioritized including at least one example of each heterocycle, although we failed to find compounds with
244 piperazine and indazole that satisfied all other selection criteria. We observed that certain heterocycles
245 (shown in Figure 4C) were overrepresented based on our selection criteria; therefore, we limited the number
246 of these structures in the SAMPL6 challenge set to at most one in each set. To achieve broad and uniform
247 sampling of the measurable $\log P$ dynamic range, we segregated the molecules into bins of predicted XlogP
248 values and selected compounds from each bin, prioritizing less expensive compounds.

249 Filtering for UV chromophores

250 The presence of UV chromophores (absorbing in the 200–400 nm range) in close proximity to protonation
251 sites is necessary for spectrophotometric pK_a measurements. To filter for molecules with UV chromophores,
252 we looked at the substructure matches to the SMARTS pattern $[n, o, c] [c, n, o] cc$ which was considered
253 the smallest unit of pi-conjugation that can constitute a UV chromophore. This SMARTS pattern describes
254 extended conjugation systems comprised of four heavy atoms and composed of aromatic carbon, nitrogen,
255 or oxygen, such as 1,3-butadiene, which possesses an absorption peak at 217 nm. Additionally, the final set
256 of selected molecules was manually inspected to make sure all potentially titratable groups were no more

257 than four heavy atoms away from a UV chromophore.

258 25 fragment-like and 10 drug-like compounds were selected, out of which procurement of 28 was
259 completed in time. pK_a measurements for 17 (SM01–SM17) and 7 (SM18–SM24) were successful, respectively.
260 The resulting set of 24 small molecules constitute the SAMPL6 pK_a challenge set. For the other four
261 compounds, UV-metric pK_a measurements show no detectable pK_a s in the range of 2–12, so we decided not
262 to include them in the SAMPL6 pK_a challenge. Experiments for these four compounds are not reported in
263 this publication.

264 Python scripts used in the compound selection process are available from GitHub [[https://github.com/
265 choderalab/sAMPL6-physicochemical-properties](https://github.com/choderalab/sAMPL6-physicochemical-properties)]. Procurement details for each compound can be found
266 in Supplementary Table 1. Chemical properties used in the selection of compounds are summarized in
267 Supplementary Table 2.

268 UV-metric pK_a measurements

269 Experimental pK_a measurements were collected using the spectrophotometric pK_a measurement method
270 with a Sirius T3 automated titrator instrument (Pion) at 25°C and constant ionic strength. The Sirius T3
271 is equipped with an Ag/AgCl double-junction reference electrode to monitor pH, a dip probe attached to
272 UV spectrophotometer, a stirrer, and automated volumetric titration capability. The Sirius T3 UV-metric
273 pK_a measurement protocol measures the change in multi-wavelength absorbance in the UV region of the
274 absorbance spectrum while the pH is titrated over pH 1.8–12.2 [28, 29]. UV absorbance data is collected
275 from 160–760 nm while the 250–450 nm region is typically used for pK_a determinations. Subsequent global
276 data analysis identifies pH-dependent populations of macrostates and fits one or more pK_a values to match
277 this population with a pH-dependent model.

278 DMSO stock solutions of each compound with 10 mg/ml concentration were prepared by weighing 1 mg
279 of powder chemical with a Sartorius Analytical Balance (Model: ME235P) and dissolving it in 100 μ L DMSO
280 (Dimethyl sulfoxide, Fisher Bioreagents, CAT: BP231-100, LOT: 116070, purity \geq 99.7%). DMSO stock solutions
281 were capped immediately to limit water absorption from the atmosphere due to the high hygroscopicity
282 of DMSO and sonicated for 5–10 minutes in a water bath sonicator at room temperature to ensure proper
283 dissolution. These DMSO stock solutions were stored at room temperature up to two weeks in capped glass
284 vials. 10 mg/ml DMSO solutions were used as stock solutions for the preparation of three replicate samples
285 for the independent titrations. For each experiment, 1–5 μ L of 10 mg/ml DMSO stock solution was delivered
286 to a 4 mL Sirius T3 glass sample vial with an electronic micropipette (Rainin EDP3 LTS 1–10 μ L). The volume
287 of delivered DMSO stock solution, which determines the sample concentration following dilution by the
288 Sirius T3, is optimized individually for each compound to achieve sufficient but not saturated absorbance
289 signal (targeting 0.5–1.0 AU) in the linear response region. Another limiting factor for sample concentration
290 was ensuring that the compound remains soluble throughout the entire pH titration range. An aliquot of
291 25 μ L of mid-range buffer (14.7 mM K_2HPO_4 and 0.15 M KCl in H_2O) was added to each sample, transferred
292 with a micropipette (Rainin EDP3 LTS 10–100 μ L) to provide enough buffering capacity in middle pH ranges
293 so that pH could be controlled incrementally throughout the titration.

294 pH is temperature and ionic-strength dependent. A peltier device on the Sirius T3 kept the analyte
295 solution at 25.0 ± 0.5 °C throughout the titration. Sample ionic strength was adjusted by dilution in 1.5 mL
296 ionic strength-adjusted water (ISA water \equiv 0.15 M KCl in H_2O) by the Sirius T3. Analyte dilution, mixing,
297 acid/base titration, and measurement of UV absorbance was automated by the Sirius T3 UV-metric pK_a
298 measurement protocol. The pH was titrated between pH 1.8 and 12.2 via the addition of acid (0.5 M HCl)
299 and base (0.5 M KOH), targeting 0.2 pH steps between UV absorbance spectrum measurements. Titrations
300 were performed under argon flow on the surface of the sample solution to limit the absorption of carbon
301 dioxide from air, which can alter the sample pH to a measurable degree. To fully capture all sources of
302 experimental variability, instead of performing three sequential pH titrations on the same sample solution,
303 three replicate samples (prepared from the same DMSO stock solution) were subjected to one round of
304 pH titration each. Although this choice reduced throughput and increased analyte consumption, it limited
305 the dilution of the analyte during multiple titrations, resulting in stronger absorbance signal for pK_a fitting.
306 Under circumstances where analyte is scarce, it is also possible to do three sequential titrations using the

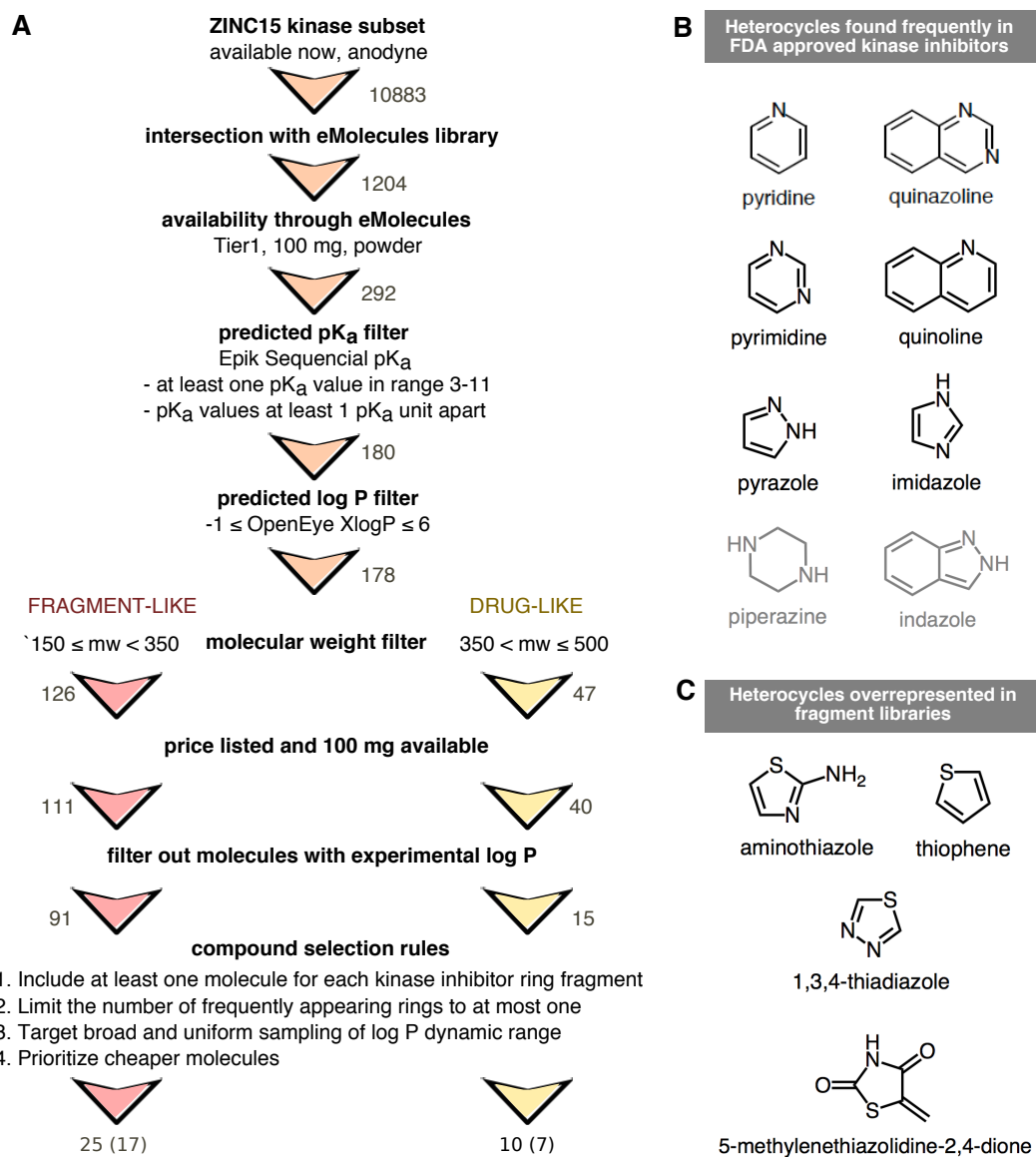


Figure 4. Compound selection for the SAMPL6 pK_a challenge, with the goal of running subsequent log P/log D challenges on the same compound set. (A) Flowchart of filtering steps for the selection of compounds that resemble kinase inhibitors and their fragments. Numbers next to arrows indicate the number of compounds remaining after each filtering step. A total of 25 fragment-like and 10 drug-like compounds were selected, out of which procurement and pK_a measurements for 17 fragment-like and 7 drug-like compounds were successful, respectively. (B) Frequent heterocycles found in FDA approved kinase inhibitors, as determined by Bemis-Murcko fragmentation into rings [49]. Black structures were represented in SAMPL6 set at least once. Compounds with piperazine and indazole (gray structures) could not be included in the challenge set due to library and selection limitations. (C) Structures of heterocycles that were overrepresented based on our compound selection workflow. We have limited the number of occurrences of these heterocycles to at most one.

307 same sample to limit consumption when the loss of accuracy is acceptable.

308 Visual inspection of the sample solutions after titration and inspection of the pH-dependent absorbance
309 shift in the 500–600 nm region of the UV spectra was used to verify no detectable precipitation occurred
310 during the course of the measurement. Increased absorbance in the 500–600 nm region of the UV spectra is
311 associated with scattering of longer wavelengths of light in the presence of colloidal aggregates. For each
312 analyte, we optimized analyte concentration, direction of the titration, and pH titration range in order to
313 maintain solubility over the entire experiment. The titration direction was specified so that each titration
314 would start from the pH where the compound is most soluble: low-to-high pH for bases and high-to-low
315 pH for acids. While UV-metric pK_a measurements can be performed with analyte concentrations as low as
316 50 μM (although this depends on the absorbance properties of the analyte), some compounds may yet not
317 be soluble at these low concentrations throughout the pH range of the titration. As the sample is titrated
318 through a wide range of pH values, it is likely that low-solubility ionization states—such as neutral and
319 zwitterionic states—will also be populated, limiting the highest analyte concentration that can be titrated
320 without encountering solubility issues. For compounds with insufficient solubility to accurately determine a
321 pK_a value directly in a UV-metric titration, a cosolvent protocol was used, as described in the next section
322 (**UV-metric pK_a measurement with cosolvent**).

323 Two Sirius T3 computer programs—Sirius T3 Control v1.1.3.0 and Sirius T3 Refine v1.1.3.0—were used
324 to execute measurement protocols and analyze pH-dependent multiwavelength spectra, respectively. Pro-
325 tonation state changes at titratable sites near chromophores will modulate the UV-absorbance spectra of
326 these chromophores, allowing populations of distinct UV-active species to be resolved as a function of pH.
327 To do this, basis spectra are identified and populations extracted via TFA analysis of the pH-dependent
328 multi-wavelength absorbance [29]. When fitting the absorbance data to a titratable molecule model to
329 estimate pK_a s, we selected the minimum number of pK_a s sufficient to provide a high-quality fit between
330 experimental and modeled data based on visual inspection of pH-dependent populations.

331 This method is capable of measuring pK_a values between 2–12 when titratable groups are at most 4–5
332 heavy atoms away from chromophores such that a change in protonation state alters the absorbance
333 spectrum of the chromophore. We selected compounds where titratable groups are close to potential
334 chromophores (generally aromatic ring systems), but the possibility exists that our experiments did not
335 detect protonation state changes of titratable groups distal from UV chromophores.

336 **Cosolvent UV-metric pK_a measurements of molecules with poor aqueous solubilities**

337 If analytes are not sufficiently soluble during the titration, pK_a values cannot be accurately determined via
338 aqueous titration directly. If precipitation occurs, the UV-absorbance signal from pH-dependent precipitate
339 formation cannot be differentiated from the pH-dependent signal of soluble microstate species. For com-
340 pounds with low aqueous solubility, pK_a values were estimated from multiple apparent pK_a measurements
341 performed in ISA methanol:ISA water cosolvent solutions with various mole fractions, from which the pK_a
342 at 0% methanol (100% ISA water) can be extrapolated. This method is referred to as a UV-metric p_sK_a
343 measurement in the Sirius T3 Manual [51]. p_sK_a value is the apparent pK_a value measured in the presence
344 of a cosolvent.

345 The cosolvent spectrophotometric pK_a measurement protocol was very similar to the standard aqueous
346 UV-metric pK_a measurement protocol, with the following differences: titrations were performed in typically
347 in 30%, 40%, and 50% mixtures of ISA methanol:ISA water by volume to measure apparent pK_a values (p_sK_a)
348 in these mixtures. Yasuda-Shedlovsky extrapolation [52, 53] was subsequently used to estimate the pK_a
349 value at 0% cosolvent (Figure 5) [31, 54, 55].

$$p_sK_a + \log[\text{H}_2\text{O}] = A/\epsilon + B \quad (1)$$

350 Yasuda-Shedlovsky extrapolation relies on the linear correlation between $p_sK_a + \log[\text{H}_2\text{O}]$ and the reciprocal
351 dielectric constant of the cosolvent mixture ($1/\epsilon$). In Eq. 1, A and B are the slope and intercept of the line
352 fitted to experimental datapoints. Depending on the solubility requirements of the analyte, the methanol
353 ratio of the cosolvent mixtures was adjusted. We designed the experiments to have at least 5% cosolvent

354 ratio difference between datapoints and no more than 60% methanol content. Calculation of the Yasuda-
355 Shedlovsky extrapolation was performed by the Sirius T3 software using at least 3 $p_s K_a$ values measured in
356 different ratios of methanol:water. Addition of methanol (80%, 0.15 M KCl) was controlled by the instrument
357 before each titration. Three consecutive pH titrations at different methanol concentrations were performed
358 using the same sample solution. In addition, three replicate measurements with independent samples
359 (prepared from the same DMSO stock) were collected.

360 **Calculation of uncertainty in pK_a measurements**

361 Experimental uncertainties were reported as the standard error of the mean (SEM) of three replicate pK_a
362 measurements. The standard error of the mean (SEM) was estimated as

$$\text{SEM} = \frac{\sigma}{\sqrt{N}} \quad ; \quad \sigma = \sqrt{\frac{1}{N} \sum_{i=1}^N (x_i - \mu)^2} \quad ; \quad \mu = \frac{1}{N} \sum_{i=1}^N x_i \quad (2)$$

363 where σ denotes the sample standard deviation and μ denotes the sample mean. x_i are observations and N
364 is the number of observations.

365 Since the Sirius T3 software reports pK_a values to only two decimal places, we have reported the SEM
366 as 0.01 in cases where SEM values calculated from 3 replicates were lower than 0.01. SEM calculated from
367 replicate measurements were found to be larger than non-linear fit error reported by the Sirius T3 Refine
368 Software from UV-absorbance model fit of a single experiment, thus leading us to believe that running
369 replicate measurements and reporting mean and SEM of pK_a measurements is better for capturing all
370 sources of experimental uncertainty. Notably, for UV-metric measurements, the measured pK_a values
371 should be insensitive to final analyte concentration and any uncertainty in the exact analyte concentration of
372 the original DMSO stock solution, justifying the use of the same stock solution (rather than independently
373 prepared stock solutions) for multiple replicates.

374 **Quality control for chemicals**

375 Compound purity was assessed by LC-MS using an Agilent HPLC 1200 Series equipped with auto-sampler,
376 UV diode array detector, and a Quadrupole MS detector 6140. ChemStation version C01.07SR2 was used
377 to analyze LC & LC/MS. An Ascentis Express C18 column (3.0 x 100 mm, 2.7 μm) was used, with column
378 temperature set at 45° C.

- 379 • Mobile phase A: 2 mM ammonium formate (pH = 3.5) aqueous
- 380 • Mobile phase B: 2 mM ammonium formate in 90:10 acetonitrile:water (pH = 3.5)
- 381 • Flow rate : 0.75 ml/min
- 382 • Gradient: Starting with 10% B to 95% B in 10 minutes then hold at 95% B for 5 minutes.
- 383 • Post run length: 5 minutes
- 384 • Mass condition: ESI positive and negative mode
- 385 • Capillary voltage: 3000 V
- 386 • Drying gas flow: 12 ml/min
- 387 • Nebulizer pressure: 35 psi
- 388 • Drying temperature: 350°C
- 389 • Mass range: 5-1350 Da; Fragmentor: 70; Threshold: 100

390 The percent area for the primary peak is calculated based on the area of the peak divided by the total
391 area of all peaks. The percent area of the primary peak is reported as an estimate of sample purity. The
392 purity of primary LC peak was checked by ChemStation software with threshold 995, to check that there is
393 no significant impurity underneath the main peak.

394 **NMR determination of protonation microstates**

395 In general, the chemical shifts of nuclear species observed in nuclear magnetic resonance (NMR) spectra
396 report on and are very sensitive to the chemical environment. Consequently, small changes in chemical

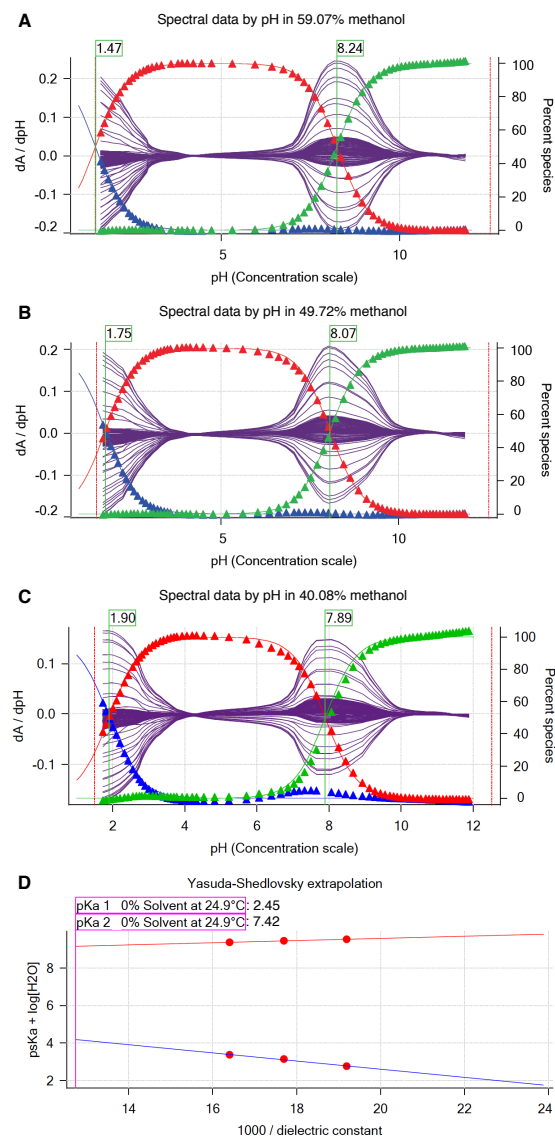


Figure 5. Determination of SM22 pK_a values with cosolvent method and Yasuda-Shedlovsky extrapolation. **A**, **B**, and **C** show p_sK_a of SM22 determined at various methanol concentrations: 59.07%, 49.72%, 40.08% by weight. Purple solid lines indicate the derivative of the absorbance signal with respect to pH vs pH at multiple wavelengths. p_sK_a values (green flags) were determined by Sirius T3 Refine Software. Blue, red, and green triangles show relative populations of macroscopic protonation states with respect to pH calculated from the experimental data. Notice that as cosolvent concentration increases, p_sK_{a1} decreases from 1.90 to 1.47 and p_sK_{a2} increases from 7.84 to 8.24. **D** Yasuda-Shedlovsky extrapolation plot for SM22. Red datapoints correspond to p_sK_a determined at various cosolvent ratios. Based on linear fitting to $p_sK_a + \log[H_2O]$ vs $1/\epsilon$, pK_{a1} and pK_{a2} in 0% cosolvent (aqueous solution) was determined as 2.45 and 7.42, respectively. R^2 values of linear fits are both 0.99. The slope of Yasuda-Shedlovsky extrapolation shows if the observed titration has acidic (positive slope) or basic (negative slope) character dominantly, although this is an macroscopic observation and should not be relied on for annotation of pK_a s to functional groups (microscopic pK_a s).

397 environment, such as the protonation events described in this work, are manifest as changes in the chemical
398 shift(s) of the nuclei. If perturbation occurs at a rate which is fast on the NMR timescale (*fast exchange*),
399 an average chemical shift is observed. This phenomena has been exploited and utilized as a probe for
400 determining the order of protonation for molecules with more than one titratable site [56]. In some
401 cases, direct observation of the titrated nuclei can be difficult, for example nitrogen and oxygen, due to
402 sample limitations and/or low natural abundance of the NMR active nuclei (0.37% for ^{15}N and 0.038% for
403 ^{17}O)—amongst other factors. In these situations, chemical shifts changes of the so-called “reporter” NMR
404 nuclei— ^1H , ^{31}P , or ^{13}C nuclei, which are directly attached to or are a few bonds away from the titrated
405 nuclei—have been utilized as the probe for NMR-pH titrations [21, 57, 58]. This approach is advantageous
406 since the sensitive NMR nuclides (^1H and ^{31}P) are observed. In addition, ^{31}P and ^{13}C offer large spectral
407 widths of ~ 300 ppm and ~ 200 ppm, respectively, which minimize peak overlap.

408 However, reporter nuclei chemical shifts provide indirect information subject to interpretation. In complex
409 systems with multiple titratable groups, such analysis will be complicated due to a cumulative effect of these
410 groups on the reporter nuclide due to their close proximity or the resonance observed in aromatic systems.
411 In contrast, direct observation of the titratable nuclide where possible, affords a more straight-forward
412 approach to studying the protonation events. In this study, the chemical shifts of the titratable nitrogen
413 nuclei were observed using the ^1H - ^{15}N -HMBC (Heteronuclear Multiple-Bond Correlation) experiments — a
414 method that affords the observation of ^{15}N chemical shifts while leveraging the sensitivity accrued from the
415 high abundance the ^1H nuclide.

416 The structures of samples SM07 and SM14 were assigned via a suite of NMR experiments, which included
417 ^1H NMR, ^{13}C NMR, homonuclear correlated spectroscopy (^1H - ^1H COSY), heteronuclear single quantum
418 coherence (^1H - ^{13}C HSQC), ^{13}C heteronuclear multiple-bond correlation (^1H - ^{13}C -HMBC) and ^{15}N heteronuclear
419 multiple-bond correlation (^1H - ^{15}N -HMBC)—see SI. All NMR data used in this analysis were acquired on a
420 Bruker 500 MHz spectrometer equipped with a 5 mm TCI CryoProbeTM Prodigy at 298 K. The poor solubility
421 of the analytes precluded analysis in water and thus water- d_2 /methanol- d_4 mixture and acetonitrile- d_3 were
422 used as solvents. The basic sites were then determined by titration of the appropriate solutions of the
423 samples with equivalent amounts of deuterio-trifluoroacetic acid (TFA-*d*) solution.

424 SM07

425 5.8 mg of SM07 was dissolved in 600 μL of methanol- d_4 :water- d_2 (2:1 v/v ratio). A 9% v/v TFA-*d* solution in
426 water- d_2 was prepared, such that each 20 μL volume contained approximately 1 equivalent of TFA-*d* with
427 respect to the base. The SM07 solution was then titrated with the TFA-*d* solution at 0.5, 1.0, 1.5, and 5.0
428 equivalents with ^1H - ^{15}N HMBC spectra (optimized for 5 Hz) acquired after each TFA addition. A reference
429 ^1H - ^{15}N HMBC experiment was first acquired on the SM07 solution prior to commencement of the titration.

430 SM14

431 5.5 mg of SM14 was dissolved in 600 μL of acetonitrile- d_3 . A 10% v/v TFA-*d* solution in acetonitrile- d_3 was
432 prepared, 20 μL of which corresponds to 1 equivalent of TFA-*d* with respect to the base. Further 1:10 dilution
433 of the TFA-*d* solution in acetonitrile- d_3 , allowed measurement of 0.1 equivalent of TFA-*d* per 20 μL of solution.
434 The SM14 solution was then titrated with the TFA-*d* solutions at 0.0, 0.5, 1.0, 1.1, 1.2, 1.3, 1.5, 1.8, 2.0, 2.1, 2.6,
435 5.1, and 10.1 equivalents. The chemical shift changes were monitored by the acquisition of ^1H - ^{15}N HMBC
436 spectra (optimized for 5 Hz) after each TFA addition.

437 Results

438 Spectrophotometric pK_a measurements

439 Spectrophotometrically-determined pK_a values for all molecules from the SAMPL6 pK_a challenge are shown
440 in Figure 6 and Table 1. The protocol used—cosolvent or aqueous UV-metric titration—is indicated in
441 Table 1 together with SEM of each reported measurement. Out of 24 molecules successfully assayed, five
442 molecules have two resolvable pK_a values, while one has three resolvable pK_a values within the measurable
443 pK_a range of 2–12. The SEM of reported pK_a measurements is low, with the largest uncertainty reported
444 being 0.04 pK units (pK_{a1} of SM06 and pK_{a3} of SM18). Individual replicate measurements can be found in

Table 1. Experimental pK_a s of SAMPL6 compounds. Spectrophotometric pK_a measurements were performed with two assay types based on aqueous solubility of analytes. "UV-metric pK_a " assay indicates spectrophotometric pK_a measurements done with Sirius T3 in ISA water. "UV-metric pK_a with cosolvent" assay refers to pK_a determination by Yasuda-Shedlovsky extrapolation from p_sK_a measurements in various ratios of ISA methanol:water mixtures. Triplicate measurements were performed at $25.0 \pm 0.5^\circ$ C and in the presence of approximately 150 mM KCl to adjust ionic strength.

Molecule ID	pK_{a1}	pK_{a2}	pK_{a3}	Assay Type
SM01	9.53 ± 0.01			UV-metric pK_a
SM02	5.03 ± 0.01			UV-metric pK_a with cosolvent
SM03	7.02 ± 0.01			UV-metric pK_a with cosolvent
SM04	6.02 ± 0.01			UV-metric pK_a
SM05	4.59 ± 0.01			UV-metric pK_a with cosolvent
SM06	3.03 ± 0.04	11.74 ± 0.01		UV-metric pK_a
SM07	6.08 ± 0.01			UV-metric pK_a
SM08	4.22 ± 0.01			UV-metric pK_a
SM09	5.37 ± 0.01			UV-metric pK_a with cosolvent
SM10	9.02 ± 0.01			UV-metric pK_a with cosolvent
SM11	3.89 ± 0.01			UV-metric pK_a
SM12	5.28 ± 0.01			UV-metric pK_a
SM13	5.77 ± 0.01			UV-metric pK_a
SM14	2.58 ± 0.01	5.30 ± 0.01		UV-metric pK_a
SM15	4.70 ± 0.01	8.94 ± 0.01		UV-metric pK_a
SM16	5.37 ± 0.01	10.65 ± 0.01		UV-metric pK_a
SM17	3.16 ± 0.01			UV-metric pK_a
SM18	2.15 ± 0.02	9.58 ± 0.03	11.02 ± 0.04	UV-metric pK_a with cosolvent
SM19	9.56 ± 0.02			UV-metric pK_a with cosolvent
SM20	5.70 ± 0.03			UV-metric pK_a with cosolvent
SM21	4.10 ± 0.01			UV-metric pK_a with cosolvent
SM22	2.40 ± 0.02	7.43 ± 0.01		UV-metric pK_a with cosolvent
SM23	5.45 ± 0.01			UV-metric pK_a with cosolvent
SM24	2.60 ± 0.01			UV-metric pK_a with cosolvent

¹ pK_a values are reported as mean \pm SEM of three replicates.

445 Supplementary Table 3. Reports generated for each pK_a measurement by the Sirius T3 Refine software can
446 also be found in the Supplementary Information. Experimental pK_a values for nearly all compounds with
447 multiple resolvable pK_a s are well-separated (more than 4 pK_a units), except for SM14 and SM18.

448 **Impact of cosolvent to UV-metric pK_a measurements**

449 For molecules with insufficient aqueous solubilities throughout the titration range (pH 2–12), we resorted
450 to cosolvent UV-metric pK_a measurements, with methanol used as cosolvent. To confirm that cosolvent
451 UV-metric pK_a measurements led to indistinguishable results compared to aqueous UV-metric measure-
452 ments, we collected pK_a values of 12 highly soluble SAMPL6 compounds—as well as pyridoxine—using
453 both cosolvent and aqueous methods. Correlation analysis of pK_a values determined with both methods
454 demonstrated that using methanol as cosolvent and determining aqueous pK_a s via Yasuda-Shedlovsky
455 extrapolation did not result in significant bias (Figure 7), since 95% CI for mean deviation (MD) between
456 two measurements includes zero. Means and standard errors of UV-metric pK_a measurements with and
457 without cosolvent are provided in Supplementary Table 5. pK_a measurement results of individual replicate
458 measurements with and without cosolvent can be found in Supplementary Table 4.

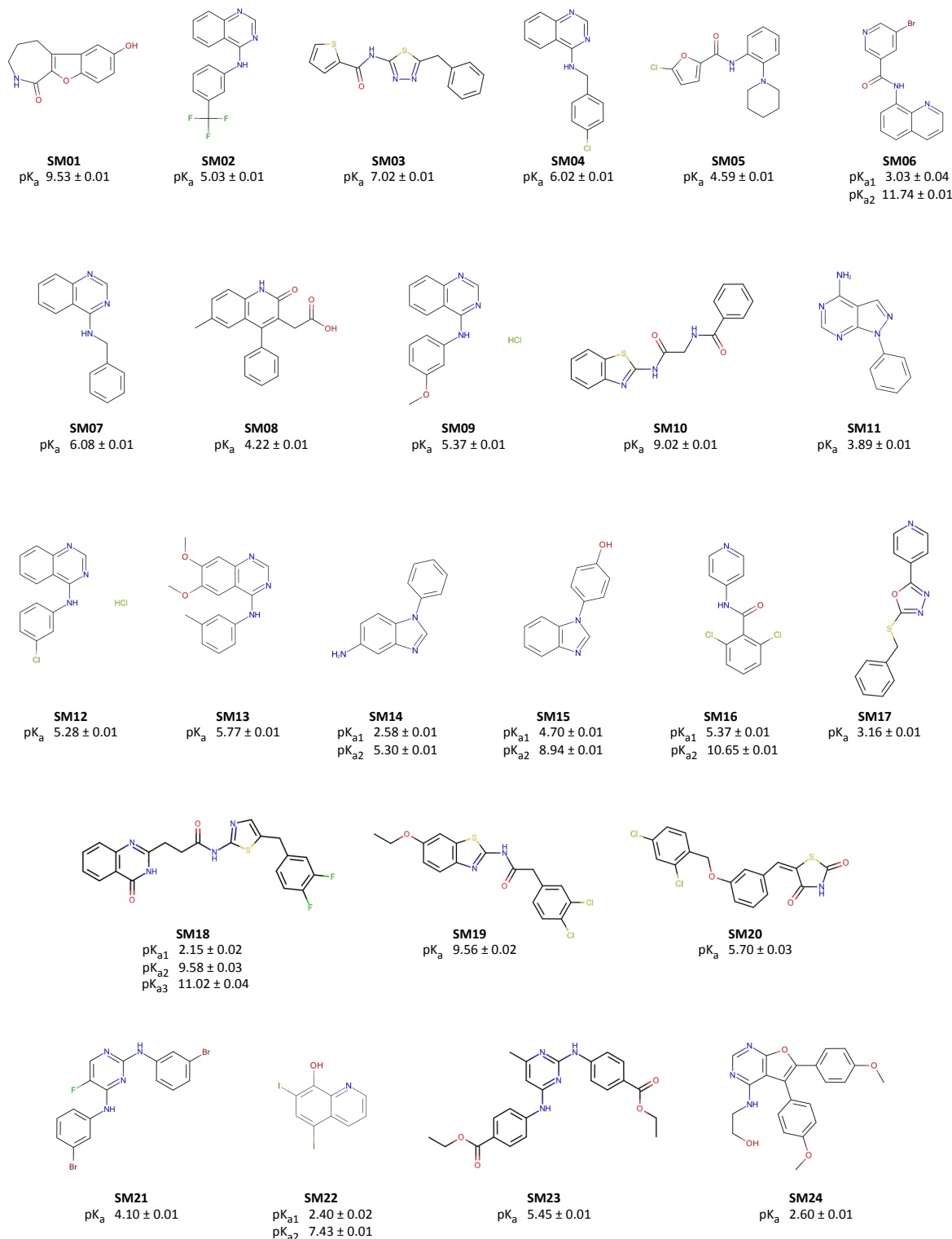


Figure 6. Molecules used in the SAMPL6 pK_a challenge. Experimental UV-metric pK_a measurements were performed for these 24 molecules and discernable macroscopic pK_as are reported. Uncertainties are expressed as the standard error of the mean (SEM) of three independent measurements. We depicted neutral states of the molecules as sites of protonation were not determined by UV-metric methods. 2D structures were created with OpenEye OEDEPict Toolkit [59]. Canonical isomeric SMILES of molecules in this figure and pK_a values measured in replicate experiments can be found in Table SI 1 and Table SI 3, respectively.

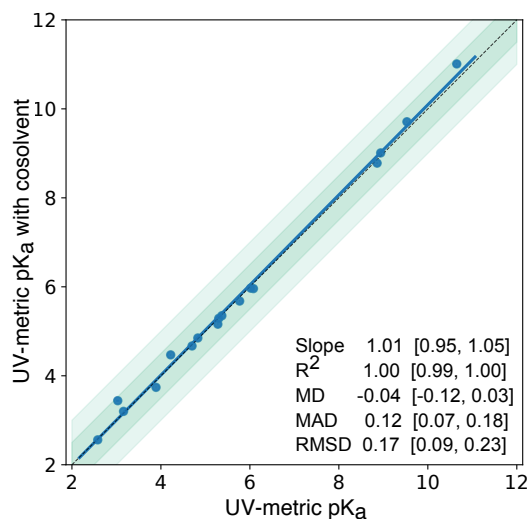


Figure 7. pK_a measurements with UV-metric method with cosolvent and UV-metric method in water show good correlation. 17 pK_a values (blue marks) of 13 chemicals were measured with both UV-metric pK_a method in water and UV-metric pK_a method with methanol as cosolvent (Yasuda-Shedlovsky extrapolation to 0% methanol). Dashed black line has slope of 1, representing perfect correlation. Dark and light green shaded areas indicate ± 0.5 and ± 1.0 pK_a unit difference regions, respectively. Error bars are plotted as the SEM of replicate measurements, although they are not visible since the largest SEM is 0.04. MD: Mean difference, MAD: Mean absolute deviation, RMSD: Root-mean-square deviation. Confidence intervals (reported in brackets) report the 95%ile CI calculated over 10 000 bootstrap samples. Experimental data used in this plot is reported in Supplementary Table 4.

459 Purity of SAMPL6 compounds

460 LC-MS based purity measurements showed that powder stocks of 23 of the SAMPL6 pK_a challenge com-
461 pounds were >90% pure, while purity of SM22 was 87%—the lowest in the set (Supplementary Table 6). Addi-
462 tionally, molecular weights detected by LC-MS method were consistent with those reported in eMolecules,
463 as well as supplier-reported molecular weights, when provided. It is recommended by Sirius/Pion technical
464 specialists to use compounds with ~90% purity to minimize the impact on high-accuracy pK_a measurements.
465 Impurities with no UV-chromophore, or elute too late in LC may not be detected with this method, although
466 chances are small. The peak purity check of primary peak can detect the presence of a large impurity
467 underneath the main peak, but if the UV spectrum of the impurity is exactly same with analyte in the main
468 peak, it may not be resolved. HPLC UV detector's wavelength inaccuracy is <1%. Mass inaccuracy of MS
469 instrument is ~0.13 um within the calibrated mass range in the scan mode.

470 Characterization of SM07 microstates with NMR

471 ¹⁵N Chemical shifts (ppm, referenced to external liquid ammonia at 0 ppm) for N-8, N-10 and N-12—measured
472 from the ¹H-¹⁵N HMBC experiments—were plotted against the titrated TFA-*d* equivalents (0.0, 0.5, 1.0, 1.5,
473 and 5.0 equivalents) (Figure 8 A). A large upfield shift of ~82 ppm is observed for N-12. The initial linear
474 relationship between chemical shift and TFA equivalents, shown in Figure 8A for N-12, is expected for strong
475 monoprotic bases—as is the case for SM07. The large upfield chemical shift change (82 ppm) is consistent
476 with a charge delocalization as shown in the resonance structures in Figure 8A. Further evidence for this
477 delocalization is observed for N-8, which exhibited a downfield chemical shift change of ~28 ppm compared
478 to just ~1.5 ppm for N-10. Titration of SM07 with more than 1 equivalent of TFA-*d* did not result in further
479 significant chemical shift changes—establishing that SM07 is a monoprotic base.

480 **Characterization of SM14 microstates with NMR**

481 Determining the protonation sites for SM14, which has pK_a values of 2.58 and 5.30 (Table 1), was more
482 challenging due to multiple possible resonance structures in the mono- and di-protonated states. We
483 noticed that the water/methanol co-solvent exhibited strong solvent effects, which complicated the data
484 interpretation for SM14. For instance, titration of SM14 in methanol/water (Figure SI 36) showed incomplete
485 protonation of N-9 even after 5 equivalents of TFA-*d* were added. This observation is consistent with UV-
486 metric p_sK_a measurements done in the presence of methanol as cosolvent, where both p_sK_a values were
487 decreasing as the percentage of methanol was increased, making observation of these protonation states
488 more difficult. Thus the utilization of an aprotic solvent was necessary for unambiguous interpretation of
489 the data.

490 Due to the problem just delineated for the methanol/water cosolvent, acetonitrile- d_3 was selected as
491 our solvent of choice. Titration of SM14 (5.5 mg) with up to 10 equivalents of TFA-*d* in acetonitrile- d_3 (0.0,
492 0.5, 1.0, 1.1, 1.2, 1.3, 1.5, 1.8, 2.0, 2.1, 2.6, 5.1, and 10.1 equivalents), provided a much clearer picture of its
493 protonation states (Figure 8 B). N-9, with the large upfield chemical shift change ~ 72 ppm at 1 equivalent
494 of TFA-*d*, clearly is the site of first protonation. Concurrently, the downfield chemical shift changes were
495 observed for N-7 ($\Delta\delta \approx 6.5$) and N-16 ($\Delta\delta \approx 5$) that can be attributed to electronic effects rather than a
496 direct protonation. The large upfield shift for N-9 indicates this to be the site of first protonation; complete
497 protonation was attained at roughly 2.5 equivalents of TFA-*d*, suggesting that SM14 is a weak base under
498 these experimental conditions. Following the protonation of N-9, a second protonation event occurs at N-16
499 nitrogen as evident by the upfield chemical shift change observed for N-16. However, a continuous change
500 in the chemical shift of N-16 even after addition of 10 equivalents of TFA-*d* indicates that this protonation
501 event is incomplete but provides evidence for N-16 being the second protonation site. This observation is
502 consistent with N-16 being even a weaker base than N-9, which is expected of the aniline-type amines. Other
503 notable observations were the slight downfield chemical shift changes for N-7 and N-9, during the second
504 protonation event. These changes were attributed to electronic effects from the protonation of N-16.

505 **Discussion**

506 **Effect of sample preparation and cosolvents in UV-metric measurements**

507 Samples for UV-metric pK_a measurements were prepared by dilution of up to 5 μ L DMSO stock solution
508 of analyte in 1.5 mL ISA water, which results in the presence of $\sim 0.3\%$ DMSO during titration, which is
509 presumed to have a negligible effect on pK_a measurements. For UV-metric or pH-metric measurements, it is
510 possible to prepare samples without DMSO, but it is difficult to prepare samples by weighing extremely low
511 amounts of solid stocks (in the order of 0.01–0.10 mg) to target 50 μ M analyte concentrations, even with
512 an analytical balance. For experimental throughput, we therefore preferred using DMSO stock solutions.
513 Another advantage of starting from DMSO stock solutions is that it helps to overcome kinetic solubility
514 problems of analytes.

515 A lower analyte concentration is needed for spectrophotometric pK_a measurement than potentiometric
516 method. With spectrophotometric method, very dilute analyte solutions as low as 10^{-5} – 10^{-6} M can be
517 used [28] with strength of the UV signal as limiting factor. In this study we used analyte concentrations
518 around 50 μ M, which is 2 orders of magnitude lower than the minimum concentration required for typical
519 potentiometric pK_a measurements. Theoretically, low analyte concentrations lead to more accurate pK_a
520 measurements by minimizing the potential for the solute to influence solvent properties. In the extreme,
521 if it were possible to measure the pK_a at the infinite dilution of the analyte that would be the best. But of
522 course, in practice the minimum analyte concentration is limited by the detection strength of the UV signal.
523 The higher the analyte concentration the more it affects the solvent properties such as ionic strength and
524 dielectric constant. Also, the risk of analyte aggregation or precipitation increases with higher concentration.

525 In UV-metric measurements, both water and methanol (when used as cosolvent) stock solutions were
526 ionic strength adjusted with 150 mM KCl, but acid and base solutions were not. This means that throughout
527 pH titration ionic strength slightly fluctuates, but on average ionic strength of samples were staying around
528 150–180 mM. By using ISA solutions the effect of salt concentration change on pK_a measurements was

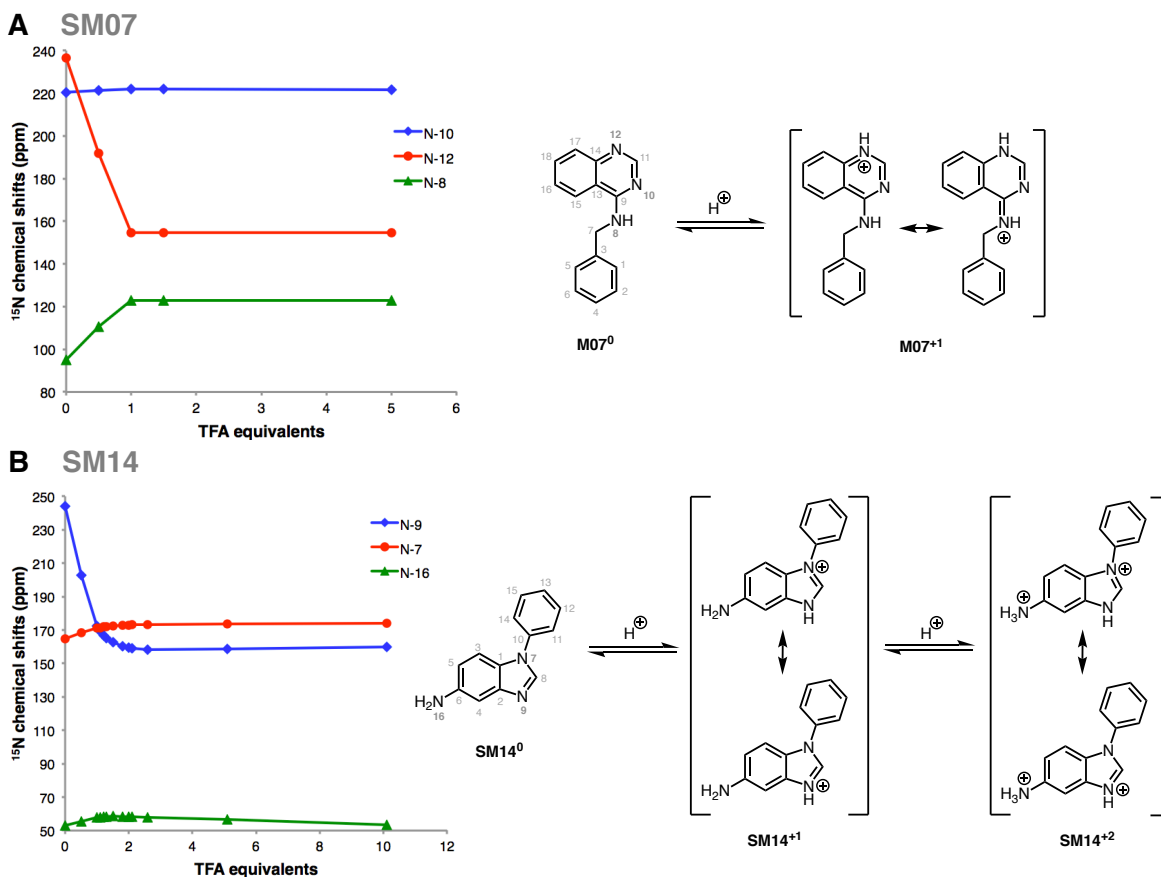


Figure 8. Dominant protonation microstates of SM07 and SM14 characterized by NMR. (A) Sequence of protonation sites of SM07 were determined by ^1H - ^{15}N HMBC experiments in 1:2 water:methanol mixture. *Left:* The plot of ^{15}N chemical shifts of the N-10, N-12, and N-8 resonances of SM07 vs titrated TFA-*d* equivalents, showing the mono-protonation of N-12 as evidenced by its large upfield chemical shifts change. Acidity of the medium increased as more equivalents of TFA-*d* were added. Electronic effects due to protonation of N-12 caused downfield chemical shift change of N-10 and N-8 between 0–1 equivalents of TFA-*d*. *Right:* NMR-based model of the order of dominant protonation states for SM07. The protonation event was only observed at N-12. Microstates shown in the figure are the most likely contributors to the UV-metric $\text{p}K_a$ of 6.08 ± 0.01 . (B) Sequence of protonation sites of SM14 were determined by ^1H - ^{15}N HMBC experiments in acetonitrile. *Left:* The plot of ^{15}N chemical shifts of N-9, N-7, and N-16 of SM14 vs titrations of TFA-*d* equivalents, showing two sequential protonation events. The first protonation occurred at N-9; a large upfield chemical shift change of 71.6 ppm was seen between 0–1 equivalents of TFA-*d*. Downfield chemical shift changes observed for N-7 and N-19 in this region were due the electronic effect from the protonation of N-9. N-16 also exhibited a small upfield chemical shift change of 4.4 ppm between 2.5–10 equivalents of TFA-*d*, which indicated N-16 as the second site of protonation. *Right:* NMR based model of the order of dominant protonation states for SM14, showing two sequential protonation events. Also, two $\text{p}K_a$ values were detected with UV-metric $\text{p}K_a$ measurements for SM14. Assuming that the sequence of protonation events will be conserved between water and acetonitrile solvents, SM14⁰ and SM14⁺¹ microstates shown in the figure are the major contributors to the UV-metric $\text{p}K_a$ value 5.30 ± 0.01 . SM14⁺¹ and SM14⁺² microstates shown in the figure are the major pair of microstates contributing to the UV-metric $\text{p}K_a$ value 2.58 ± 0.01 . There could be minor microstates with very low populations that could not be distinguished in these NMR experiments.

529 minimized.

530 If an analyte is soluble enough, UV-metric pK_a measurements in water should be preferred over cosolvent
531 methods, since pK_a measurement in water is more direct. For pK_a determination via cosolvent extrapolation
532 using methanol, the apparent pK_a s (p_sK_a) in at least three different methanol:water ratios must be measured,
533 and the pK_a in 0% cosolvent computed by Yasuda-Shedlovsky extrapolation. The number and spread of
534 p_sK_a measurements and error in linear fit extrapolation influences the accuracy of pK_a s determined by this
535 approach. To test that UV-metric methods with or without cosolvent have indistinguishable performance,
536 we collected pK_a values for 17 SAMPL6 compounds and pyridoxine with both methods. Figure 7 shows there
537 is good correlation between both methods and the mean absolute deviation between two methods is 0.12
538 (95% CI [0.07, 0.18]). The mean deviation between the two sets is -0.04 (95% CI [-0.12, 0.03]), showing there is
539 no significant bias in cosolvent measurements as the 95% CI includes zero. The largest absolute deviation
540 observed was 0.41 for SM06.

541 **Impact of impurities to UV-metric pK_a measurements**

542 Precisely how much the presence of small amounts of impurities impact UV-metric pK_a measurements is
543 unpredictable. For an impurity to alter UV-metric pK_a measurements, it must possess a UV-chromophore and
544 a titratable group in the vicinity of the chromophore—otherwise, it would not interfere with absorbance signal
545 of the analyte. If a titratable impurity *does* possess a UV-chromophore, UV multiwavelength absorbance
546 from the analyte and impurity will be convoluted. How much the presence of impurity will impact the
547 multiwavelength absorbance spectra and pK_a determination depends on the strength of the impurity's molar
548 absorption coefficient and concentration, relative to the analyte's. In the worst case scenario, an impurity
549 with high concentration or strong UV absorbance can shift the measured pK_a value or create the appearance
550 of an extra pK_a . As a result, it is important to use analytes with high purities to obtain high accuracy pK_a
551 measurements. Therefore, we confirmed the purities of SAMPL6 compounds with LC-MS.

552 **Interpretation of UV-metric pK_a measurements**

553 Multiwavelength absorbance analysis on the Sirius T3 allows for good resolution of pK_a s based on UV-
554 absorbance change with respect to pH, but it is important to note that pK_a values determined from this
555 method are often difficult to assign as either microscopic or macroscopic in nature. This method potentially
556 produces *macroscopic* pK_a s for polyprotic compounds. If multiple microscopic pK_a s have close pK_a values
557 and overlapping changes in UV absorbance spectra associated with protonation/deprotonation, the spectral
558 analysis could produce a single macroscopic pK_a that represents an aggregation of multiple microscopic pK_a s.
559 An extreme example of such case is demonstrated in the simulated macrostate populations of cetirizine that
560 would be observed with UV-metric titration (Figure 2).

561 If protonation state populations observed via UV-metric titrations (such as in Figure 3B) are composed
562 of a single microstate, experimentally measured pK_a s are indeed microscopic pK_a s. Unfortunately, judging
563 the composition of experimental populations is not possible by just using UV-metric or pH-metric titration.
564 Molecules in the SAMPL6 pK_a challenge dataset with only one pK_a value measured in the 2–12 range could
565 therefore be monoprotic (possessing a single titratable group that changes protonation state by gain or
566 loss of a single proton over this pH range) or polyprotic (gaining or losing multiple protons from one or
567 more sites with overlapping microscopic pK_a values). Similarly, titration curves of molecules with multiple
568 experimental pK_a s may show well-separated microscopic pK_a s or macroscopic experimental pK_a s that
569 are really composites of microscopic pK_a s with similar values. Therefore, without additional experimental
570 evidence, UV-metric pK_a s should not be assigned to individual titratable groups.

571 Sometimes it can be possible to assign pK_a s to ionizable groups if they produce different UV-absorbance
572 shifts upon ionization, but it is not a straight-forward analysis and it is not a part of the analysis pipeline of
573 Sirius T3 Refine Software. Such an analysis would require fragmentation of the molecule and determining
574 how UV-spectra of each chromophore changes upon ionization in isolation.

575 UV-metric pK_a values for nearly all compounds in our dataset with multiple resolvable pK_a s are well-
576 separated (more than 4 pK_a units), except for SM14 and SM18. Tam et al. states that spectrophotometric
577 pK_a values of multiprotic molecules can be unambiguously assigned to the functional groups as microscopic

578 pK_a s "if the pK_a values are at least 4 pH units apart (i.e. $pK_{a,2} - pK_{a,1} \geq 4$)" based on general knowledge of
579 functional groups and consideration of electronic and inductive effects [28]. In this study, we refrained from
580 reporting such a knowledge-based assignment of pK_a values to functional groups without experimental
581 evidence.

582 Determination of the exact microstates populated at different pH values via NMR can provide a com-
583plementary means of differentiating between microscopic and macroscopic pK_a s in cases where there is
584ambiguity. As determination of protonation microstates via NMR is very laborious, we were only able to
585characterize microstates of two molecules: SM07 and SM14.

586 In UV-metric pK_a measurements with cosolvent, the slope of the Yasuda-Shedlovsky extrapolation can
587be interpreted to understand if the pK_a has dominantly acidic or basic character. As the methanol ratio
588is increased, p_sK_a values of acids increase, while p_sK_a values for bases decrease. However, it is important
589to remember that if the measured pK_a is macroscopic, acid/base assignment from cosolvent p_sK_a trends
590is also a macroscopic property, and should not be used as a guide for assigning pK_a values to functional
591groups [60].

592 NMR microstate characterization

593 The goal of NMR characterization was to collect information on microscopic states related to experimental
594 pK_a measurements, i.e., determine exact sites of protonation. pK_a measurements performed with spec-
595trophotometric method provide macroscopic pK_a values, but do not provide information on the specific
596site(s) of protonation. Conversely, most computational prediction methods primarily predict microscopic
597 pK_a values. Protonation sites can be determined by NMR methods, although these measurements are
598very laborious in terms of data collection and interpretation compared to pK_a measurements with the
599automated Sirius T3. Moreover, not all SAMPL6 molecules were suitable for NMR measurements due to
600the high sample concentration requirements (for methods other than proton NMR, such as ^{13}C and ^{15}N
601based 2D experiments) and limiting analyte solubility. Heavy atom spectra that rely on natural isotope
602abundance require high sample concentrations (preferably in the order of 100 mM). It is possible that drug
603or drug-fragment-like compounds, such as the compounds used in this study, have insufficient aqueous
604solubility, limiting the choice of solvent and pH. It may be necessary to use organic cosolvents to prepare
605these high concentration solutions or only prepare samples at pH values that correspond to high solubility
606states (e.g., when the charged state of the compound is populated).

607 We performed NMR based microstate characterization only for SM07 and SM14. We were able to identify
608the order of dominant protonation microstates, as shown in Figure 8. These pairs of microstates and
609the order of microscopic transitions can be associated with experimental pK_a s determined by UV-metric
610titrations, under the assumption that different organic solvents used in NMR measurements will have
611negligible effect on the sequence of microstates observed as the medium was titrated with acid, although
612shift in pK_a values is expected. NMR measurements for SM07 and SM14 were done in water:methanol
613(1:2 (v/v)) and acetonitrile solutions, respectively. On the other hand, pK_a values of these two compounds
614were determined by UV-metric titrations in ISA water. Additional UV-metric pK_a measurements of these
615compounds with methanol as a cosolvent showed that their p_sK_a values decreased as the cosolvent ratio
616increased (i.e., dielectric constant decreased) as expected from base titration sites. Identification of SM07
617and SM14 titratable sites type as base is consistent between NMR based models and UV-metric cosolvent
618titrations. The order of microstates observed in the titration of NMR samples are very likely to corresponds
619to the dominant microstates associated with UV-metric pK_a measurements. N-12 of SM07 was observed as
620the only protonation site of SM07 during TFA-*d* titration up to 5 equivalents which supports that SM07 is
621mono-protic and UV-metric pK_a value 6.08 ± 0.01 corresponds to microscopic protonation of N-12. For SM14,
622two protonation sites were observed (N-16 and N-9, in the order of increasing p_sK_a). Microstate pairs shown
623in Figure 8B were determined as dominant contributors to UV-metric pK_a s 2.58 ± 0.01 and 5.30 ± 0.01 , although
624minor microspecies with very low populations (undetected in NMR experiments) could be contributing to
625the macroscopic pK_a values observed by the UV-metric method.

626 In addition to SM07, there were five other 4-aminoquinazoline derivatives in the SAMPL6 set: SM02, SM04,
627 SM09, SM12, and SM13. For these series, all the potential titratable sites are located in 4-aminoquinazoline

628 scaffold and there are no other additional titratable sites present in these compounds compared to SM07.
629 Therefore, based on structural similarity, it is reasonable to predict that N-12 is the microscopic protonation
630 site for all of these compounds. We can infer that UV-metric pK_a values measured for the 4-aminoquinazoline
631 series are also microscopic pK_a s and they are related to the protonation of the same quinazoline nitrogen
632 with the same neutral background protonation states as shown for SM07 in Figure 8A.

633 **Recommendations for future pK_a prediction challenges**

634 Most high-throughput pK_a measurement methods measure macroscopic pK_a s. One way to circumvent
635 this problem is to confine our interest in future pK_a challenges to experimental datasets containing only
636 monoprotic compounds if UV-metric or pH-metric pK_a measurements are the method of choice, allowing
637 unambiguous assignment of pK_a values to underlying protonation states. However, it is important to
638 consider that multiprotic compounds are common in pharmaceutically interesting molecules, necessitating
639 the ability to model them reliably. It might also be interesting to select a series of a polyprotic compounds
640 and their monoprotic fragments, to see if they can be used to disambiguate the pK_a values.

641 Although relatively efficient, UV-metric pK_a measurements with the Sirius T3 do not provide structural
642 information about microstates. Even the acid-base assignment based on direction of $p_s K_a$ shift with cosolvent
643 is not a reliable indicator for assigning experimental pK_a values to individual functional groups in multiprotic
644 compounds. On the other hand, most computational pK_a prediction methods output microscopic pK_a s.
645 It is therefore difficult to use experimental macroscopic pK_a values to assess and train microscopic pK_a
646 prediction methods directly without further means of annotating macroscopic-microscopic correspondence.
647 It is not straight-forward to infer the underlying microscopic pK_a values from macroscopic measurements
648 of a polyprotic compound without complementary experiments that can provide structural information.
649 Therefore, for future data collection efforts for evaluation of pK_a predictions, if measurement of pK_a s via
650 NMR is not possible, we advise supplementing UV-metric measurements with NMR characterization of
651 microstates to show if observed pK_a s are microscopic (related to a single group) or macroscopic (related to
652 dissociation of multiple groups), as performed for SM07 and SM14 in this study.

653 Another source of complexity in interpreting macroscopic pK_a values is how the composition of macro-
654 scopic pK_a s can change between different experimental methods as illustrated in Figure 2. Different subsets
655 of microstates can become indistinguishable based on the type of signal the experimental method is con-
656 structed on. In potentiometric titrations, microstates with the same total charge are indistinguishable
657 and are observed as one macroscopic population. In spectrophotometric pK_a measurements, the factor
658 that determine if microstates can be resolved is not charge. Instead, microstates whose populations, and
659 therefore UV-absorbance spectra, change around the same pH value become indistinguishable.

660 The "macroscopic" label is commonly ascribed to transitions between different ionization states of a
661 molecule (all microstates that have the same total charge form one macrostate), but this definition only
662 applies to potentiometric methods. In UV-absorbance based methods, the principle that determines which
663 microstates will be distinguishable is not charge or number of bound protons, but molecular absorbance
664 changes, and how closely underlying microscopic pK_a values overlap. To compare experimental macroscopic
665 pK_a and microscopic computational predictions on common ground, the best solution is to compute "pre-
666 dicted" macroscopic pK_a values from microscopic pK_a s based on the detection limitations of the experiment.
667 A disadvantage of this approach is that experimental data cannot provide direct guidance on microscopic
668 pK_a resolution for improving pK_a prediction methods.

669 Since analyte purity is critical for accuracy, necessary quality control experiments must be performed to
670 ensure at least 90% purity for UV-metric pK_a measurements. Higher purities may be necessary for other
671 methods. For potentiometric methods, knowing the stoichiometry of any counterions present in the original
672 powder stocks is also necessary. Identity of counterions also needs to be known to incorporate titratable
673 counterions, e.g. ammonia in the titration model.

674 For the set of SAMPL6 pK_a challenge compounds, we could not use potentiometric pK_a measurements
675 due to the low aqueous solubility of many of these compounds. The lowest solubility observed *somewhere*
676 in the experimental pH range of titration is the limiting factor, since for accurate measurements the analyte
677 must stay in the solution phase throughout the entire titration. Since the titration pH range is determined

678 with the goal of capturing all ionization states, the analyte is inevitably exposed to pH values that correspond
679 to low solubility. Neutral and zwitterionic species can be orders of magnitude less soluble than ionic species.
680 If a compound has a significantly insoluble ionization state, the pH range of titration could be narrowed to
681 avoid precipitation, but it would limit the range of pK_a values that could be accurately measured.

682 For future pK_a challenges with multiprotic compounds, if sufficient time and effort can be spared, it would
683 be ideal to construct an experimental pK_a dataset using experimental methods that can measure microscopic
684 pK_a s directly, such as NMR. In the present study, we were only able to perform follow up NMR microstate
685 characterization of two compounds because we relied on intrinsically low-sensitivity and time-consuming
686 ^1H - ^{15}N HMBC experiment at natural abundance of ^{15}N nuclei. ^1H - ^{15}N HMBC experiments of SM07 and SM14
687 required high analyte concentrations and thus the use of organic solvents for solubility. Alternatively, it
688 might be possible to determine microstates with ^1H -NMR by analyzing chemical shift changes of reporter
689 protons [21] in aqueous solutions with lower analyte concentrations and with much higher throughput than
690 ^{15}N -based experiments. However, it should be noted that ^1H NMR titration data may not always be sufficient
691 for unambiguous microstate characterization. In this case, other reporter nuclei such as ^{13}C , ^{19}F and ^{31}P
692 can be used where appropriate to supplement ^1H data To prepare sample solutions for NMR at specific pH
693 conditions, the Sirius T3 can be used to automate the pH adjustment of samples. Another advantage of
694 using the Sirius T3 for NMR sample preparation includes preparing ionic strength adjusted NMR samples
695 and minimizing consumption of the analyte since small volumes (as low as 1.5 mL) of pH adjusted solutions
696 can be prepared.

697 In the future pK_a challenges, it would be especially interesting to expand this exercise to larger and
698 more flexible drug-like molecules. pK_a values are environment dependent and it would be useful to be
699 able to predict pK_a shifts based on on ionic strength, temperature, lipophilic content, with cosolvents or in
700 organic solvents. Measuring the pK_a of molecules in organic solvents would be useful for guiding process
701 chemistry. To test such predictions, special pK_a experiments would need to be designed to measure pK_a s
702 under different conditions.

703 The next iteration of the SAMPL $\log D$ prediction challenge will include a subset of compounds from pK_a
704 challenge. We therefore envision that the collected dataset of pK_a measurements will also be of use for
705 this challenge. Experimental pK_a values will be provided as an input to separate the pK_a prediction issue
706 from other problems related to $\log D$ predictions. We expect that the experimental pK_a s can be used as an
707 indication if protonation states need to be taken into account for a $\log D$ prediction at a certain pH and for
708 the validation of protonation state population predictions in the aqueous phase. Even for compounds for
709 which microstates were not experimentally determined, macroscopic pK_a value can serve as an indicator of
710 how likely it is that protonation states will have a significant effect on the $\log D$ of a molecule. Additionally, the
711 information from NMR experiments in this study provided the site of protonation for six 4-aminoquinazoline
712 compounds, which could be incorporated as microstate information for $\log D$ predictions. For predicting
713 $\log D$ we suggest as a rule of thumb to include protonation state effects for pK_a values at least within 2 units
714 of the pH of the $\log D$ experiment. pK_a values of six 4-aminoquinazoline compounds in this study were
715 determined to be within 2 pK_a units from 7.

716 Conclusion

717 This study reports the collection of experimental data for the SAMPL6 pK_a prediction challenge. Collection of
718 experimental pK_a data was performed with the goal of evaluating computational pK_a predictions, therefore
719 necessary quality control and uncertainty propagation measures were incorporated. The challenge was
720 constructed for a set of fragment-like and drug-like small molecules, selected from kinase-targeted chemical
721 libraries, resulting in a set of compounds containing heterocycles frequently found in FDA-approved kinase
722 inhibitors. We collected pK_a values for 24 compounds with the Sirius T3 UV-metric titration method, which
723 were then used as the experimental reference dataset for the SAMPL6 pK_a challenge. For compounds with
724 poor aqueous solubilities we were able to use the Yasuda-Shedlovsky extrapolation method to measure pK_a
725 values in the presence of methanol, and extrapolate to a purely aqueous phase.

726 In our work, we highlighted the distinction between microscopic and macroscopic pK_a s which is based
727 on the experimental method used, especially how underlying microstate composition can be different for

728 macroscopic pK_a values measured with UV-metric vs pH-metric titration methods. We discuss how macro-
729 scopic pK_a values, determined by UV, introduce an identifiability problem when comparing to microscopic
730 computational predictions. For two compounds (SM07 and SM14) we were able to alleviate this problem by
731 determining the sequence of microscopic protonation states using ^1H - ^{15}N HMBC experiments. Microstates
732 of five other compounds with 4-aminoquinazoline scaffold were inferred based on the NMR characterization
733 of SM07 microstates which showed that it is monoprotic.

734 The collected experimental data constitute a potentially useful dataset for future evaluation of small
735 molecule pK_a predictions, even outside of SAMPL challenges. We expect that this data will also be useful for
736 participants in the next SAMPL challenge on small molecule lipophilicity predictions.

737 Code and data availability

- 738 • SAMPL6 pK_a challenge instructions, submissions, experimental data and analysis is available at
<https://github.com/MobleyLab/SAMPL6>
- Python scripts used for compound selection are available at **compound_selection** directory of
<https://github.com/choderalab/sampl6-physicochemical-properties>

739 Overview of supplementary information

740 Supplementary tables and figures appearing in SI document:

- 741 • TABLE SI 1: Procurement details of SAMPL6 compounds
- 742 • TABLE SI 2: Selection details of SAMPL6 compounds
- 743 • TABLE SI 3: pK_a results of replicate experiments CSV
- 744 • TABLE SI 4: pK_a results of water and cosolvent replicate experiments CSV
- 745 • TABLE SI 5: pK_a mean and SEM results of water and cosolvent replicate experiments
- 746 • TABLE SI 6: Summary of LC-MS purity results
- 747 • FIGURE SI 1 - 24: LC-MS Figures
- 748 • FIGURE SI 25-35: NMR characterization of SM07 microstates
- 749 • FIGURE SI 36-54: NMR characterization of SM14 microstates

750 Additional files:

- 751 • Sirius T3 reports for all measurements: `supplementary_files.zip`

752 Author Contributions

753 Conceptualization, MI, JDC, TR, ASR, DLM ; Methodology, MI, DL, IEN ; Software, MI, ASR ; Formal Analysis, MI ;
754 Investigation, MI, DL, IEN, HW, XW, MR; Resources, TR, DL; Data Curation, MI ; Writing-Original Draft, MI, JDC,
755 IEN; Writing - Review and Editing, MI, DL, ASR, IEN, HW, XW, MR, GEM, DLM, TR, JDC; Visualization, MI, IEN ;
756 Supervision, JDC, TR, DLM, GEM, AAM ; Project Administration, MI ; Funding Acquisition, JDC, DLM, TR, MI.

757 Acknowledgments

758 MI, ASR, and JDC acknowledge support from the Sloan Kettering Institute. JDC acknowledges support
759 from NIH grant P30 CA008748. MI, JDC, ASR, and DLM gratefully acknowledge support from NIH grant
760 R01GM124270 supporting SAMPL blind challenges. MI acknowledges support from a Doris J. Hutchinson
761 Fellowship. DLM appreciates financial support from the National Institutes of Health (1R01GM108889-01), the
762 National Science Foundation (CHE 1352608). IEN acknowledges support from the MRL Postdoctoral Research
763 Program. The authors are extremely grateful for the assistance and support from the MRL Preformulations
764 and NMR Structure Elucidation groups for materials, expertise, and instrument time, without which this
765 SAMPL challenge would not have been possible. MI and DL are grateful to Pion/Sirius Analytical for their
766 technical support in the planning and execution of this study. We are especially thankful to Karl Box (Sirius
767 Analytical) for the guidance on optimization and interpretation of pK_a measurements with the Sirius T3,
768 as well as feedback on the manuscript. We thank Brad Sherborne (MRL; ORCID: [0000-0002-0037-3427](https://orcid.org/0000-0002-0037-3427))
769 for his valuable insights at the conception of the pK_a challenge and connecting us with TR and DL who

770 were able to provide resources for experimental measurements. We acknowledge Paul Czodrowski (Merck
771 KGaA; ORCID: [0000-0002-7390-8795](https://orcid.org/0000-0002-7390-8795)) who provided feedback on multiple stages of this work: challenge
772 construction, purchasable compound selection, and manuscript. We acknowledge contributions from Caitlin
773 Bannan who provided feedback on experimental data collection and structure of pK_a challenge from a
774 computational chemist's perspective. We are also grateful to Marilyn Gunner (CCNY) for her feedback on
775 this manuscript. We thank anonymous reviewers for their input and constructive comments that improved
776 this manuscript. MI, ASR, and JDC are grateful to OpenEye Scientific for providing a free academic software
777 license for use in this work. The content is solely the responsibility of the authors and does not necessarily
778 represent the official views of the National Institutes of Health.

779 Disclosures

780 JDC was a member of the Scientific Advisory Board for Schrödinger, LLC during part of this study. JDC and
781 DLM are current members of the Scientific Advisory Board of OpenEye Scientific Software. The Chodera
782 laboratory receives or has received funding from multiple sources, including the National Institutes of Health,
783 the National Science Foundation, the Parker Institute for Cancer Immunotherapy, Relay Therapeutics, Entasis
784 Therapeutics, Silicon Therapeutics, EMD Serono (Merck KGaA), AstraZeneca, the Molecular Sciences Software
785 Institute, the Starr Cancer Consortium, Cycle for Survival, a Louis V. Gerstner Young Investigator Award, and
786 the Sloan Kettering Institute. A complete list of funding can be found at <http://choderalab.org/funding>.

787 References

- 788 [1] **Mobley DL**, Chodera JD, Isaacs L, Gibb BC. Advancing predictive modeling through focused development of model
789 systems to drive new modeling innovations. UC Irvine: Department of Pharmaceutical Sciences, UCI. 2016; <https://escholarship.org/uc/item/7cf8c6cr>.
- 790 [2] **Drug Design Data Resource**, SAMPL; <https://drugdesigndata.org/about/sampl>.
- 791 [3] **Nicholls A**, Mobley DL, Guthrie JP, Chodera JD, Bayly CI, Cooper MD, Pande VS. Predicting Small-Molecule Solvation
792 Free Energies: An Informal Blind Test for Computational Chemistry. *J Med Chem*. 2008 Feb; 51(4):769–779. doi:
793 [10.1021/jm070549+](https://doi.org/10.1021/jm070549+).
- 794 [4] **Guthrie JP**. A Blind Challenge for Computational Solvation Free Energies: Introduction and Overview. *J Phys Chem B*.
795 2009 Jan; 113(14):4501–4507.
- 796 [5] **Skillman AG**, Geballe MT, Nicholls A. SAMPL2 Challenge: Prediction of Solvation Energies and Tautomer Ratios. *J*
797 *Comput Aided Mol Des*. 2010 Apr; 24(4):257–258. doi: [10.1007/s10822-010-9358-0](https://doi.org/10.1007/s10822-010-9358-0).
- 798 [6] **Geballe MT**, Skillman AG, Nicholls A, Guthrie JP, Taylor PJ. The SAMPL2 Blind Prediction Challenge: Introduction and
799 Overview. *J Comput Aided Mol Des*. 2010 May; 24(4):259–279. doi: [10.1007/s10822-010-9350-8](https://doi.org/10.1007/s10822-010-9350-8).
- 800 [7] **Skillman AG**. SAMPL3: Blinded Prediction of Host–guest Binding Affinities, Hydration Free Energies, and Trypsin
801 Inhibitors. *J Comput Aided Mol Des*. 2012 May; 26(5):473–474. doi: [10.1007/s10822-012-9580-z](https://doi.org/10.1007/s10822-012-9580-z).
- 802 [8] **Geballe MT**, Guthrie JP. The SAMPL3 Blind Prediction Challenge: Transfer Energy Overview. *J Comput Aided Mol Des*.
803 2012 Apr; 26(5):489–496. doi: [10.1007/s10822-012-9568-8](https://doi.org/10.1007/s10822-012-9568-8).
- 804 [9] **Muddana HS**, Varnado CD, Bielawski CW, Urbach AR, Isaacs L, Geballe MT, Gilson MK. Blind Prediction of Host–guest
805 Binding Affinities: A New SAMPL3 Challenge. *J Comput Aided Mol Des*. 2012 Feb; 26(5):475–487. doi: [10.1007/s10822-012-9554-1](https://doi.org/10.1007/s10822-012-9554-1).
- 806 [10] **Guthrie JP**. SAMPL4, a Blind Challenge for Computational Solvation Free Energies: The Compounds Considered. *J*
807 *Comput Aided Mol Des*. 2014 Apr; 28(3):151–168. doi: [10.1007/s10822-014-9738-y](https://doi.org/10.1007/s10822-014-9738-y).
- 808 [11] **Mobley DL**, Wymer KL, Lim NM, Guthrie JP. Blind Prediction of Solvation Free Energies from the SAMPL4 Challenge. *J*
809 *Comput Aided Mol Des*. 2014 Mar; 28(3):135–150. doi: [10.1007/s10822-014-9718-2](https://doi.org/10.1007/s10822-014-9718-2).
- 810 [12] **Muddana HS**, Fenley AT, Mobley DL, Gilson MK. The SAMPL4 Host–guest Blind Prediction Challenge: An Overview. *J*
811 *Comput Aided Mol Des*. 2014 Mar; 28(4):305–317. doi: [10.1007/s10822-014-9735-1](https://doi.org/10.1007/s10822-014-9735-1).
- 812 [13] **Mobley DL**, Liu S, Lim NM, Wymer KL, Perryman AL, Forli S, Deng N, Su J, Branson K, Olson AJ. Blind Prediction
813 of HIV Integrase Binding from the SAMPL4 Challenge. *J Comput Aided Mol Des*. 2014 Mar; 28(4):327–345. doi:
814 [10.1007/s10822-014-9723-5](https://doi.org/10.1007/s10822-014-9723-5).
- 815
- 816

- 817 [14] **Yin J**, Henriksen NM, Slochower DR, Shirts MR, Chiu MW, Mobley DL, Gilson MK. Overview of the SAMPL5 Host-guest
818 Challenge: Are We Doing Better? *J Comput Aided Mol Des*. 2017; 31(1):1–19. doi: [10.1007/s10822-016-9974-4](https://doi.org/10.1007/s10822-016-9974-4).
- 819 [15] **Bannan CC**, Burley KH, Chiu M, Shirts MR, Gilson MK, Mobley DL. Blind Prediction of Cyclohexane–water Distribution
820 Coefficients from the SAMPL5 Challenge. *J Comput Aided Mol Des*. 2016 Sep; 30(11):1–18. doi: [10.1007/s10822-016-9954-8](https://doi.org/10.1007/s10822-016-9954-8).
821
- 822 [16] **Bannan CC**, Burley KH, Chiu M, Shirts MR, Gilson MK, Mobley DL. Blind prediction of cyclohexane–water distribution
823 coefficients from the SAMPL5 challenge. *Journal of Computer-Aided Molecular Design*. 2016 Nov; 30(11):927–944.
824 <http://link.springer.com/10.1007/s10822-016-9954-8>, doi: [10.1007/s10822-016-9954-8](https://doi.org/10.1007/s10822-016-9954-8).
- 825 [17] **Rustenburg AS**, Dancer J, Lin B, Feng JA, Ortwine DF, Mobley DL, Chodera JD. Measuring experimental cyclohexane-
826 water distribution coefficients for the SAMPL5 challenge. *Journal of Computer-Aided Molecular Design*. 2016 Nov;
827 30(11):945–958. <http://link.springer.com/10.1007/s10822-016-9971-7>, doi: [10.1007/s10822-016-9971-7](https://doi.org/10.1007/s10822-016-9971-7).
- 828 [18] **Pickard FC**, König G, Tofoleanu F, Lee J, Simmonett AC, Shao Y, Ponder JW, Brooks BR. Blind prediction of distribution
829 in the SAMPL5 challenge with QM based protomer and pK_a corrections. *Journal of Computer-Aided Molecular Design*.
830 2016 Nov; 30(11):1087–1100. <http://link.springer.com/10.1007/s10822-016-9955-7>, doi: [10.1007/s10822-016-9955-7](https://doi.org/10.1007/s10822-016-9955-7).
- 831 [19] **Bodner GM**. Assigning the pK_a's of polyprotic acids. *J Chem Educ*. 1986; 63(3):246.
- 832 [20] **Darvey IG**. The assignment of pK_a values to functional groups in amino acids. Wiley Online Library; 1995.
- 833 [21] **Bezençon J**, Wittwer MB, Cutting B, Smieško M, Wagner B, Kansy M, Ernst B. pK_a determination by ¹H NMR
834 spectroscopy – An old methodology revisited. *Journal of Pharmaceutical and Biomedical Analysis*. 2014 May;
835 93:147–155. <http://linkinghub.elsevier.com/retrieve/pii/S0731708513005992>, doi: [10.1016/j.jpba.2013.12.014](https://doi.org/10.1016/j.jpba.2013.12.014).
- 836 [22] **Elson EL**, Edsall JT. Raman spectra and sulfhydryl ionization constants of thioglycolic acid and cysteine. *Biochemistry*.
837 1962; 1(1):1–7.
- 838 [23] **Elbagerma MA**, Edwards HGM, Azimi G, Scowen IJ. Raman spectroscopic determination of the acidity constants of
839 salicylaldehyde in aqueous solution. *Journal of Raman Spectroscopy*. 2011 Mar; 42(3):505–511. <http://doi.wiley.com/10.1002/jrs.2716>, doi: [10.1002/jrs.2716](https://doi.org/10.1002/jrs.2716).
840
- 841 [24] **Sober HA**, Company CR. Handbook of Biochemistry: Selected Data for Molecular Biology. Handbook of Biochem-
842 istry: Selected Data for Molecular Biology, Chemical Rubber Company; 1970. <https://books.google.com/books?id=16QRAQAAMAAJ>.
843
- 844 [25] **Benesch RE**, Benesch R. The Acid Strength of the -SH Group in Cysteine and Related Compounds. *Journal of the*
845 *American Chemical Society*. 1955; 77(22):5877–5881. <https://doi.org/10.1021/ja01627a030>, doi: [10.1021/ja01627a030](https://doi.org/10.1021/ja01627a030).
- 846 [26] **Rupp M**, Korner R, V Tetko I. Predicting the pK_a of small molecules. *Combinatorial chemistry & high throughput*
847 *screening*. 2011; 14(5):307–327.
- 848 [27] **Marosi A**, Kovács Z, Béni S, Kökösi J, Noszál B. Triprotic acid–base microequilibria and pharmacokinetic sequelae of
849 cetirizine. *European Journal of Pharmaceutical Sciences*. 2009 Jun; 37(3-4):321–328. <http://linkinghub.elsevier.com/retrieve/pii/S0928098709000773>, doi: [10.1016/j.ejps.2009.03.001](https://doi.org/10.1016/j.ejps.2009.03.001).
850
- 851 [28] **Tam KY**, Takács-Novák K. Multi-wavelength spectrophotometric determination of acid dissociation constants: a
852 validation study. *Analytica chimica acta*. 2001; 434(1):157–167.
- 853 [29] **Allen RI**, Box KJ, Comer JEA, Peake C, Tam KY. Multiwavelength spectrophotometric determination of acid dissociation
854 constants of ionizable drugs. *Journal of pharmaceutical and biomedical analysis*. 1998; 17(4):699–712.
- 855 [30] **Comer JEA**, Manallack D. Ionization Constants and Ionization Profiles. In: *Reference Module in Chemistry, Molecular*
856 *Sciences and Chemical Engineering* Elsevier; 2014. <http://linkinghub.elsevier.com/retrieve/pii/B9780124095472112338>,
857 doi: [10.1016/B978-0-12-409547-2.11233-8](https://doi.org/10.1016/B978-0-12-409547-2.11233-8).
- 858 [31] **Avdeef A**, Box KJ, Comer JEA, Gilges M, Hadley M, Hibbert C, Patterson W, Tam KY. PH-metric logP 11. pK_a
859 determination of water-insoluble drugs in organic solvent–water mixtures. *Journal of pharmaceutical and biomedical*
860 *analysis*. 1999; 20(4):631–641.
- 861 [32] **Cabot JM**, Fuguet E, Rosés M, Smejkal P, Breadmore MC. Novel Instrument for Automated pK_a Determination by
862 Internal Standard Capillary Electrophoresis. *Analytical Chemistry*. 2015 Jun; 87(12):6165–6172. <http://pubs.acs.org/doi/10.1021/acs.analchem.5b00845>, doi: [10.1021/acs.analchem.5b00845](https://doi.org/10.1021/acs.analchem.5b00845).
863

- 864 [33] **Wan H**, Holmén A, N'la ag'la ard M, Lindberg W. Rapid screening of pKa values of pharmaceuticals by pressure-assisted
865 capillary electrophoresis combined with short-end injection. *Journal of Chromatography A*. 2002; 979(1-2):369–377.
- 866 [34] **Reijenga J**, van Hoof A, van Loon A, Teunissen B. Development of Methods for the Determination of pK_a Values.
867 *Analytical Chemistry Insights*. 2013 Jan; 8:ACI.S12304. <http://journals.sagepub.com/doi/10.4137/ACI.S12304>, doi:
868 [10.4137/ACI.S12304](https://doi.org/10.4137/ACI.S12304).
- 869 [35] **Sterling T**, Irwin JJ. ZINC 15 – Ligand Discovery for Everyone. *Journal of Chemical Information and Modeling*. 2015
870 Nov; 55(11):2324–2337. <http://pubs.acs.org/doi/10.1021/acs.jcim.5b00559>, doi: [10.1021/acs.jcim.5b00559](https://doi.org/10.1021/acs.jcim.5b00559).
- 871 [36] **Baell JB**, Holloway GA. New Substructure Filters for Removal of Pan Assay Interference Compounds (PAINS) from
872 Screening Libraries and for Their Exclusion in Bioassays. *Journal of Medicinal Chemistry*. 2010 Apr; 53(7):2719–2740.
873 <http://pubs.acs.org/doi/abs/10.1021/jm901137j>, doi: [10.1021/jm901137j](https://doi.org/10.1021/jm901137j).
- 874 [37] **Saubern S**, Guha R, Baell JB. KNIME Workflow to Assess PAINS Filters in SMARTS Format. Comparison of RDKit and
875 Indigo Cheminformatics Libraries. *Molecular Informatics*. 2011 Oct; 30(10):847–850. [http://doi.wiley.com/10.1002/](http://doi.wiley.com/10.1002/minf.201100076)
876 [minf.201100076](https://doi.org/10.1002/minf.201100076), doi: [10.1002/minf.201100076](https://doi.org/10.1002/minf.201100076).
- 877 [38] eMolecules Database Free Version;. Accessed: 2017-06-01. [https://www.emolecules.com/info/](https://www.emolecules.com/info/products-data-downloads.html)
878 [products-data-downloads.html](https://www.emolecules.com/info/products-data-downloads.html).
- 879 [39] OEChem Toolkit 2017.Feb.1;. OpenEye Scientific Software, Santa Fe, NM. <http://www.eyesopen.com>.
- 880 [40] **Shelley JC**, Cholleti A, Frye LL, Greenwood JR, Timlin MR, Uchimaya M. Epik: a software program for pK_a prediction
881 and protonation state generation for drug-like molecules. *Journal of Computer-Aided Molecular Design*. 2007 Dec;
882 21(12):681–691. <http://link.springer.com/10.1007/s10822-007-9133-z>, doi: [10.1007/s10822-007-9133-z](https://doi.org/10.1007/s10822-007-9133-z).
- 883 [41] Schrödinger Release 2016-4: Epik Version 3.8;. Schrödinger, LLC, New York, NY, 2016.
- 884 [42] OEMolProp Toolkit 2017.Feb.1;. OpenEye Scientific Software, Santa Fe, NM. <http://www.eyesopen.com>.
- 885 [43] **Wishart DS**. DrugBank: a comprehensive resource for in silico drug discovery and exploration. *Nucleic Acids*
886 *Research*. 2006 Jan; 34(90001):D668–D672. <https://academic.oup.com/nar/article-lookup/doi/10.1093/nar/gkj067>,
887 doi: [10.1093/nar/gkj067](https://doi.org/10.1093/nar/gkj067).
- 888 [44] **Pence HE**, Williams A. ChemSpider: An Online Chemical Information Resource. *Journal of Chemical Education*. 2010
889 Nov; 87(11):1123–1124. <http://pubs.acs.org/doi/abs/10.1021/ed100697w>, doi: [10.1021/ed100697w](https://doi.org/10.1021/ed100697w).
- 890 [45] NCI Open Database, August 2006 Release;. <https://cactus.nci.nih.gov/download/nci/>.
- 891 [46] Enhanced NCI Database Browser 2.2;. <https://cactus.nci.nih.gov/ncidb2.2/>.
- 892 [47] **Kim S**, Thiessen PA, Bolton EE, Chen J, Fu G, Gindulyte A, Han L, He J, He S, Shoemaker BA, Wang J, Yu B, Zhang J,
893 Bryant SH. PubChem Substance and Compound databases. *Nucleic Acids Research*. 2016 Jan; 44(D1):D1202–D1213.
894 <https://academic.oup.com/nar/article-lookup/doi/10.1093/nar/gkv951>, doi: [10.1093/nar/gkv951](https://doi.org/10.1093/nar/gkv951).
- 895 [48] NCI/CADD Chemical Identifier Resolver;. <https://cactus.nci.nih.gov/chemical/structure>.
- 896 [49] **Bemis GW**, Murcko MA. The properties of known drugs. 1. Molecular frameworks. *Journal of medicinal chemistry*.
897 1996; 39(15):2887–2893.
- 898 [50] OEMedChem Toolkit 2017.Feb.1;. OpenEye Scientific Software, Santa Fe, NM. <http://www.eyesopen.com>.
- 899 [51] Sirius T3 User Manual, v1.1. Sirius Analytical Instruments Ltd, East Sussex, UK; 2008.
- 900 [52] **Yasuda M**. Dissociation constants of some carboxylic acids in mixed aqueous solvents. *Bulletin of the Chemical*
901 *Society of Japan*. 1959; 32(5):429–432.
- 902 [53] **Shedlovsky T**. The behaviour of carboxylic acids in mixed solvents. In: Pesce B, editor. *Electrolytes* New York:
903 Pergamon Press; 1962.p. 146–151.
- 904 [54] **Avdeef A**, Comer JEA, Thomson SJ. pH-Metric log P. 3. Glass electrode calibration in methanol-water, applied to
905 pKa determination of water-insoluble substances. *Analytical Chemistry*. 1993; 65(1):42–49. [https://doi.org/10.1021/](https://doi.org/10.1021/ac00049a010)
906 [ac00049a010](https://doi.org/10.1021/ac00049a010), doi: [10.1021/ac00049a010](https://doi.org/10.1021/ac00049a010).
- 907 [55] **Takács-Novák K**, Box KJ, Avdeef A. Potentiometric pKa determination of water-insoluble compounds: validation
908 study in methanol/water mixtures. *International Journal of Pharmaceutics*. 1997; 151(2):235 – 248. [http://www.](http://www.sciencedirect.com/science/article/pii/S0378517397049077)
909 [sciencedirect.com/science/article/pii/S0378517397049077](https://doi.org/10.1016/S0378-5173(97)04907-7), doi: [https://doi.org/10.1016/S0378-5173\(97\)04907-7](https://doi.org/10.1016/S0378-5173(97)04907-7).

- 910 [56] **Szakacs Z**, Beni S, Varga Z, Orfi L, Keri G, Noszal B. Acid-Base Profiling of Imatinib (Gleevec) and Its Fragments. *Journal*
911 *of Medicinal Chemistry*. 2005; 48(1):249–255. <https://doi.org/10.1021/jm049546c>, doi: 10.1021/jm049546c, pMID:
912 15634018.
- 913 [57] **Szakacs Z**, Kraszni M, Noszal B. Determination of microscopic acid?base parameters from NMR?pH titrations. *Analyt-*
914 *ical and Bioanalytical Chemistry*. 2004 Mar; 378(6):1428–1448. <http://link.springer.com/10.1007/s00216-003-2390-3>,
915 doi: 10.1007/s00216-003-2390-3.
- 916 [58] **Dozol H**, Blum-Held C, Guédât P, Maechling C, Lanners S, Schlewer G, Spiess B. Inframolecular acid–base studies of
917 the tris and tetrakis myo-inositol phosphates including the 1, 2, 3-trisphosphate motif. *Journal of molecular structure*.
918 2002; 643(1-3):171–181.
- 919 [59] OEDepict Toolkit 2017.Feb.1;. OpenEye Scientific Software, Santa Fe, NM. <http://www.eyesopen.com>.
- 920 [60] **Fraczkiewicz R**. In Silico Prediction of Ionization. In: *Reference Module in Chemistry, Molecular Sciences and Chemical*
921 *Engineering* Elsevier; 2013.<http://linkinghub.elsevier.com/retrieve/pii/B978012409547202610X>, doi: 10.1016/B978-0-
922 12-409547-2.02610-X.